Cell Reports
Medicine

Article

TRPM2 overactivation drives hyperlipidemia-induced dysfunction of myeloid cells and neurovascular units

Graphical abstract

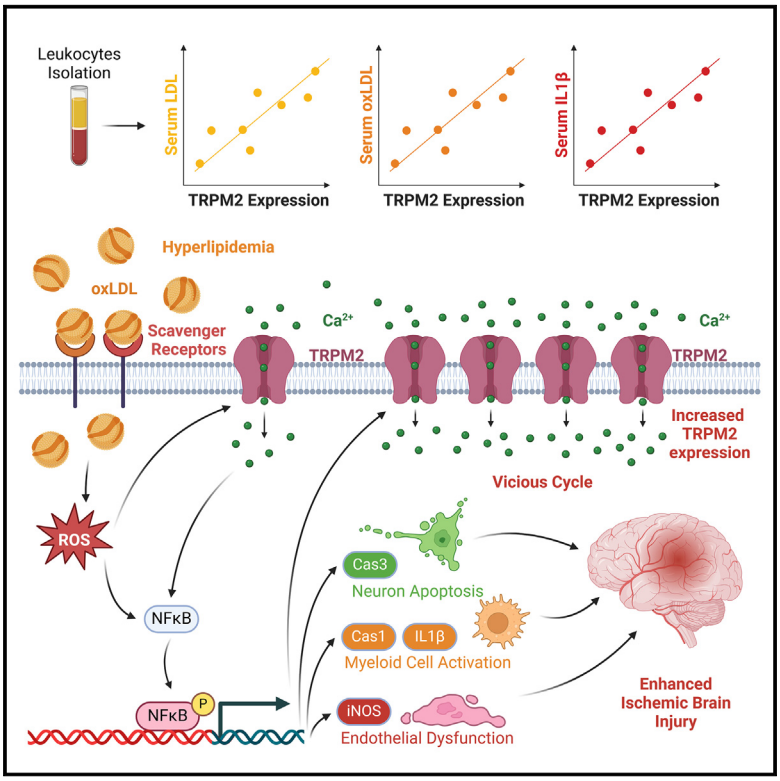

Highlights

- TRPM2 in peripheral leukocytes correlates with plasma lipid levels in humans
- TRPM2 drives the abnormal activation of peripheral leukocytes induced by lipids
- Hyperlipidemia upregulates TRPM2 expression, enhancing ischemic vulnerability
- TRPM2 inhibition mitigates ischemic stroke aggravated by hyperlipidemia

Authors

Pengyu Zong, Cindy Li, Jianlin Feng, ..., Rajkumar Verma, Bruce Liang, Lixia Yue

Correspondence

zong@uchc.edu (P.Z.),
lyue@uchc.edu (L.Y.)

In brief

Zong et al. reveal that, in humans, TRPM2 expression in peripheral leukocytes strongly correlates with plasma lipid levels. Hyperlipidemia-induced TRPM2 upregulation drives abnormal leukocyte activation, compromising vascular and neuronal resistance to ischemia. TRPM2 inhibition or cell-specific knockouts in myeloid and endothelial cells mitigate hyperlipidemia-aggravated stroke in mice.

Zong et al., 2025, Cell Reports Medicine 6, 101998
March 18, 2025
https://doi.org/10.1016/j.xcrm.2025.101998

CellPress

Cell Reports Medicine

CellPress
OPEN ACCESS

Article

TRPM2 overactivation drives hyperlipidemia-induced dysfunction of myeloid cells and neurovascular units

Pengyu Zong,[1,2,3,*] Cindy Li,[1,2,3] Jianlin Feng,[1,2] Zhichao Yue,[1,2] Nicholas Legere,[1,2,4,5] Albert S. Yu,[1,2] Fahad Shah,[1] Adrianna Perez,[1] Zhu Li,[6] Evan Jellison,[6] Yasuo Mori,[7] Barbara Miller,[8] Rajkumar Verma,[9] Bruce Liang,[1] and Lixia Yue[1,2,10,*]

[1]Calhoun Cardiology Center, University of Connecticut School of Medicine (UConn Health), 263 Farmington Avenue, Farmington, CT 06030, USA
[2]Department of Cell Biology, University of Connecticut School of Medicine (UConn Health), 263 Farmington Avenue, Farmington, CT 06030, USA
[3]Connecticut Institute for the Brain and Cognitive Sciences, University of Connecticut, 337 Mansfield Road, Unit 1272, Storrs, CT 06269, USA
[4]The Jackson Laboratory for Genomic Medicine, Farmington, CT, USA
[5]Department of Genetics and Genome Sciences, UConn Health, Farmington, CT 06030, USA
[6]Department of Immunology, University of Connecticut School of Medicine (UConn Health), Farmington, 263 Farmington Avenue, CT 06030, USA
[7]Laboratory of Molecular Biology, Department of Synthetic Chemistry and Biological Chemistry, Graduate School of Engineering, Kyoto University, Kyoto 615-8510, Japan
[8]Departments of Biochemistry and Molecular Biology, The Pennsylvania State University College of Medicine, P.O. Box 850, Hershey, PA 17033, USA
[9]Department of Neuroscience, University of Connecticut School of Medicine (UConn Health), 263 Farmington Avenue, Farmington, CT 06030, USA
[10]Lead contact
*Correspondence: zong@uchc.edu (P.Z.), lyue@uchc.edu (L.Y.)
https://doi.org/10.1016/j.xcrm.2025.101998

SUMMARY

Hyperlipidemia induces cellular dysfunction and is strongly linked to various diseases. The transient receptor potential channel melastatin 2 (TRPM2) plays a critical role in endothelial injury, immune cell activation, and neuronal death. We reveal that TRPM2 expression in human peripheral leukocytes strongly correlates with plasma lipid levels. In middle-aged *Apoe*$^{-/-}$ mice, global, myeloid, and endothelial TRPM2 knockout or TRPM2 inhibition abolishes the hyperlipidemia-induced exacerbation of ischemic brain injury suggesting that TRPM2 overactivity caused by hyperlipidemia predisposes these cells to dysfunction during ischemia. Using a clinically relevant ischemic brain injury mouse model, we demonstrate TRPM2's pivotal role in mediating hyperlipidemia's detrimental effects on myeloid cells and neurovascular units. Our findings suggest that TRPM2 is a promising therapeutic target for alleviating neurodegenerative diseases exacerbated by hyperlipidemia, such as ischemic stroke. These results also highlight TRPM2 expression in peripheral blood as a potential biomarker for predicting stroke outcomes in hyperlipidemic patients.

INTRODUCTION

Hyperlipidemia is a prevalent condition affecting over 50%–70% of adults in the developed countries, with a significant proportion of patients having a poor management of their elevated blood lipid levels.[1–3] This condition is strongly associated with many diseases, particularly myocardial infarction and ischemic stroke,[4] the leading causes of disability and mortality. Beyond being a risk factor, elevated blood lipids also directly contribute to many pathological changes. For example, during ischemic brain injury, hyperlipidemia promotes oxidative stress, endothelial dysfunction, inflammatory infiltration, and neuronal loss,[4] while high-intensity lipid-lowering therapy has demonstrated efficacy in reducing the overall incidence of strokes in individuals with recent stroke history.[5] However, the precise mechanisms through which hyperlipidemia triggers these pathological changes remain elusive, which is primarily due to the inadequate inclusion of hyperlipidemia and examination of its effects in animal models.[4] Thus, this study aims to use an ischemic stroke model in hyperlipidemic mice to investigate and elucidate the detrimental effects of hyperlipidemia on cellular dysfunctions.

Ischemic stroke is characterized by a complex pathological process involving ischemia, blood-brain-barrier (BBB) leakage, and immune cell infiltration, all of which contribute to neuronal death.[6] Despite substantial recent advances in the understanding of stroke pathophysiology, a common limitation of most current stroke

studies is their lack of clinical relevance.[7] In human stroke patients, individuals are typically middle-aged or elderly with multiple predisposed conditions, especially hyperlipidemia, hypertension, diabetes, and obesity, collectively referred to as metabolic syndrome.[8] In contrast, current animal studies often use young mice without any existing risk factors, significantly limiting the translational value of these studies.[7] This limitation may explain why therapeutic treatments always fail to attenuate ischemic stroke in human patients, despite exhibiting potent protective effects in mouse models.[7]

Transient receptor potential channel melastatin 2 (TRPM2) is a Ca^{2+}-permeable nonselective cation channel ubiquitously expressed in various tissues and cell types with varying abundance.[9] TRPM2 is recognized as a cellular sensor for oxidative stress and promotes endothelial injury, immune cell invasion, and neuronal death, thus worsening ischemic brain injury.[10,11] Previously, we showed that myeloid cell-specific TRPM2 knockout protected mice against atherogenesis induced by high-fat diet (HFD), suggesting a potential involvement of TRPM2 in hyperlipidemia-induced pathological changes.[12] However, it is unclear whether TRPM2 is involved in the exacerbation of ischemic brain injury induced by hyperlipidemia. Additionally, although TRPM2 modulators have exhibited promising therapeutic effect against ischemic stroke in mice, it remains unknown whether they will still be effective in more clinically relevant ischemic stroke models. Thus, we aimed to investigate the contribution of TRPM2 to ischemic brain injury in *Apoe*$^{-/-}$ mice, which typically develop severe hyperlipidemia and other metabolic disorders following HFD treatment,[13,14] to gain translational insight into TRPM2 inhibition in ischemic stroke and to provide a better mouse model that mimics stroke pathophysiology in humans.

RESULTS

TRPM2 expression in peripheral leukocytes correlates with blood lipids and interleukin-1β levels

TRPM2 has been well established to be required for immune cell activation,[15] and we have previously demonstrated that myeloid cell-specific TRPM2 knockout protected mice against atherogenesis induced by HFD.[12] Given that hyperlipidemia is associated with increased monocyte lipid accumulation and activation in human individuals,[16,17] our study aimed to investigate whether hyperlipidemia influences TRPM2 expression in peripheral leukocytes. We enrolled 66 middle-aged to elderly individuals and initially examined correlations between plasma levels of different blood lipids. As expected, plasma total cholesterol levels showed a positive correlation with triglyceride (Figure S1A), low-density lipoprotein (LDL) (Figure S1B), and high-density lipoprotein (HDL) (Figure S1C) levels. However, we did not find a significant correlation between LDL and triglycerides (Figure S1D) or HDL (Figure S1E), possibly due to the limited sample size.

To reliably compare the relative protein expression level of TRPM2 in peripheral leukocytes among different individuals, we normalized the TRPM2 expression to an individual with a relatively high TRPM2 level (Figure S1F). We observed no significant difference in TRPM2 expression among individuals of different age groups (Figure S1G), genders (Figures S1H [Interestingly, the elderly female enrolled in this study have higher LDL levels] and S1I), and races (Figures S1J and S1K). Subsequently, we investigated the correlations between TRPM2 expression in peripheral leukocytes and plasma levels of different lipids. We observed a weak positive correlation between TRPM2 expression and total cholesterol levels (Figure 1A). No significant correlation was found between TRPM2 expression and triglyceride levels (Figure 1B) or HDL levels (Figure 1C). However, there was a stronger correlation between TRPM2 expression and LDL levels (Figure 1D) compared to total cholesterol, suggesting that the association between TRPM2 and blood lipids is primarily contributed by LDL rather than triglyceride and HDL.

Next, we categorized individuals into four groups based on their LDL levels: optimal (less than 100 mg/dL), near optimal (100–129 mg/dL), borderline high (130–159 mg/dL), and high (more than 160 mg/dL). We observed a significant difference in TRPM2 expression between the LDL optimal and high groups, but no significant difference between LDL optimal, near optimal, or borderline high groups (Figure 1F). We also examined whether lipid-lowering therapies affect TRPM2 expression in peripheral leukocytes. Interestingly, individuals receiving high-intensity statin therapy (80 mg atorvastatin equivalent dose) exhibited significantly lower TRPM2 expression in peripheral leukocytes, despite no significant difference in LDL levels between the two groups (Figure 1G). However, there was no significant difference between individuals receiving ezetimibe and control group (Figure 1H). Considering high-intensity lipid-lowering therapy has demonstrated efficacy in reducing the risk of major adverse cardiovascular events compared to non-high-intensity statins,[18,19] our results suggest that high-intensity lipid-lowering therapy may modulate the functions of peripheral leukocytes.

We then investigated whether TRPM2 expression is correlated with systemic inflammation, which is usually seen in hyperlipidemia.[19] We found a significant correlation between circulating oxidized low-density lipoprotein (oxLDL) and total cholesterol levels (Figure 1I). Specifically, there was no significant correlation between plasma oxLDL and triglyceride levels (Figure 1J) or HDL levels (Figure 1K) but a stronger correlation between plasma oxLDL and LDL levels (Figure 1L) when compared to total cholesterol levels. Importantly, there was a significant correlation between plasma oxLDL levels and TRPM2 expression in peripheral leukocytes (Figure 1M). Circulating interleukin (IL)-1β, a marker for systemic inflammation, has been shown to be elevated in individuals with hyperlipidemia.[20] We found no significant correlation between plasma IL-1β levels and total cholesterol (Figure 1N), triglyceride (Figure S1L), or HDL (Figure S1M) levels. However, there was a significant correlation between plasma IL-1β and LDL levels (Figure 1O). Additionally, there was a stronger correlation between plasma IL-1β and oxLDL levels compared to total cholesterol and LDL (Figure 1P), suggesting that LDL and oxLDL are major contributors to systemic inflammation in hyperlipidemia. Notably, we observed an even stronger correlation between plasma IL-1β and TRPM2 expression in peripheral leukocytes (Figure 1Q). We also validated the correlation between TRPM2 expression in peripheral leukocytes and plasma levels of total cholesterol, LDL, oxLDL, and IL-1β, but not with triglyceride or HDL levels, using absolute TRPM2 expression levels measured by ELISA. (Figures S2A–S2F).

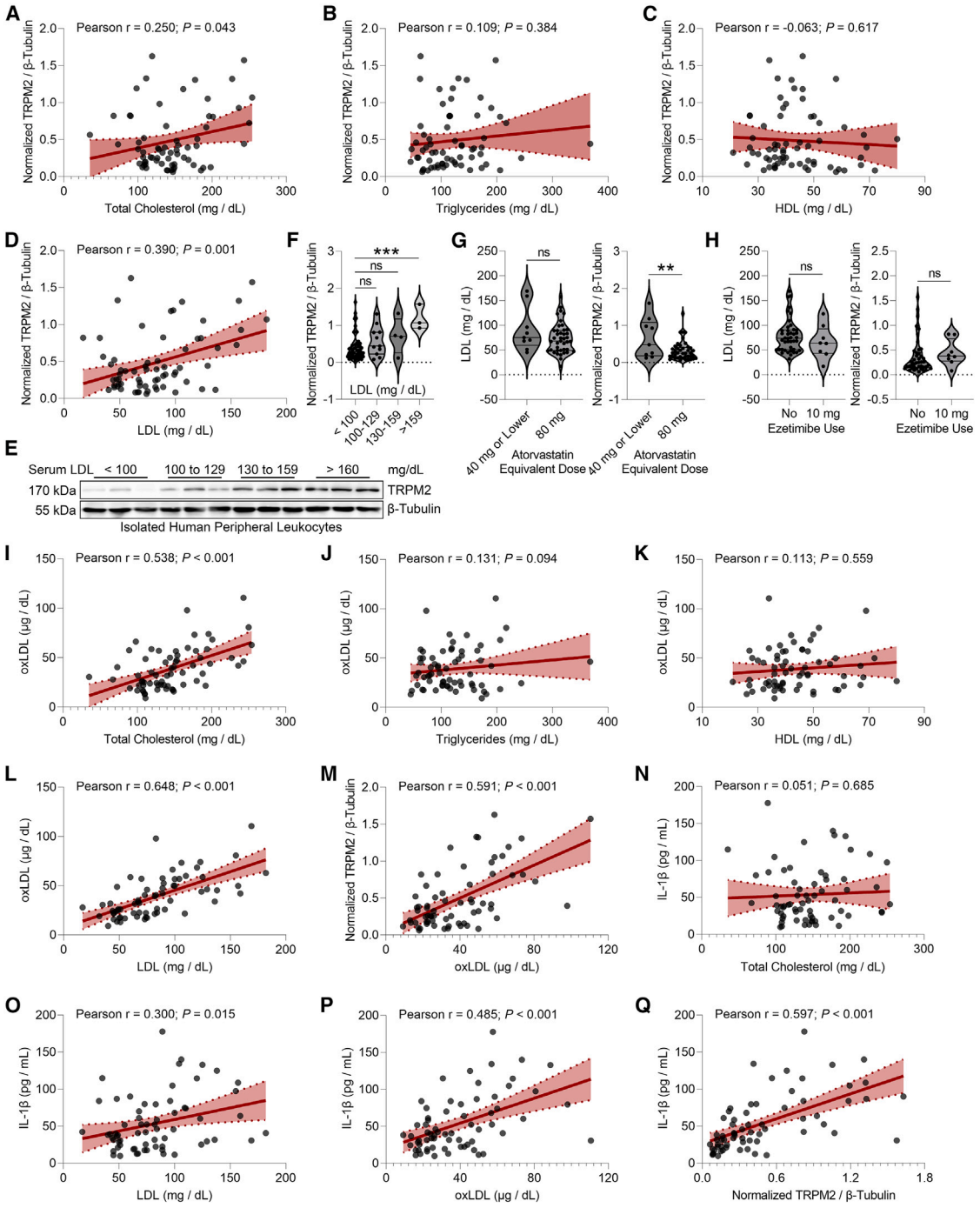

Figure 1. TRPM2 expression in peripheral leukocytes correlates with blood lipids and IL-1β levels

(A–D) Correlation of TRPM2 expression in peripheral leukocytes with total cholesterol (A), triglyceride (B), HDL (C), and LDL (D) levels in the plasma (n = 66 human individuals).

(E and F) TRPM2 expression (n = 48, 11, 4, and 3 human individuals).

(G) LDL-TRPM2 correlation in patients receiving low-moderate-intensity and high-intensity dosage statins (n = 9 and 57 human individuals).

(H) LDL-TRPM2 correlation in peripheral leukocytes in patients receiving ezetimibe or not (n = 8 and 58 human individuals).

(I–M) Correlation of plasma oxLDL level with total cholesterol (I), triglyceride (J), HDL (K), and LDL (L) levels in the plasma and TRPM2 expression in peripheral leukocytes (M) (n = 66 human individuals).

(N–Q) Correlation of plasma oxLDL level with total cholesterol (N), LDL (O), and oxLDL (P) levels in the plasma and TRPM2 expression in peripheral leukocytes (Q) (n = 66 human individuals).

Error bars: mean ± SEM; ns, no statistical significance, **, $p < 0.01$. See also Figures S1 and S2.

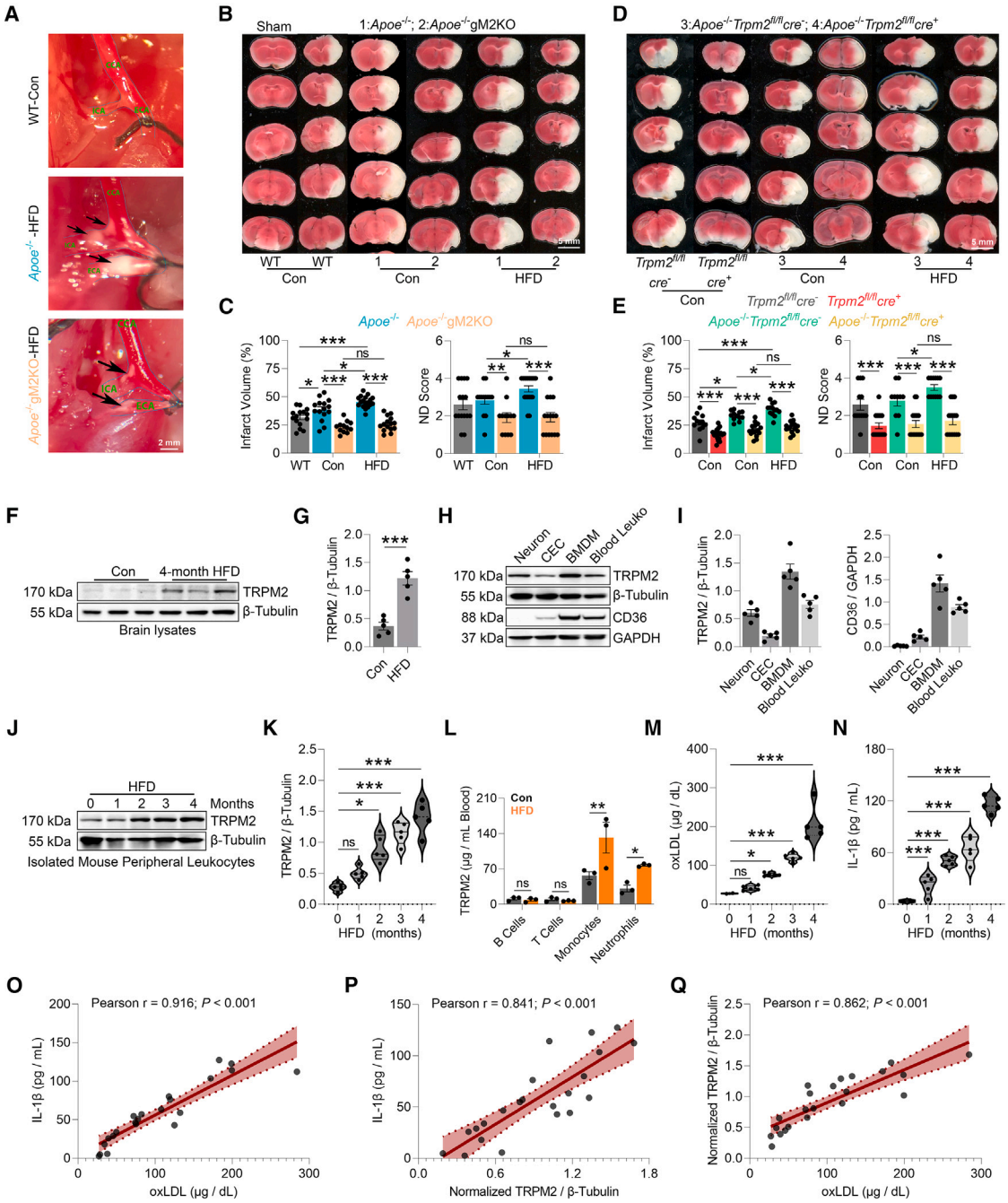

Figure 2. Global TRPM2 knockout abolishes the exacerbation of ischemic brain injury by hyperlipidemia

(A) The presence of atherosclerotic plaque (indicated by black arrows) at the bifurcation of common carotid artery (CCA) and in the internal carotid artery (ICA) (scale bar size: 2 mm).

(B–E) Triphenyl tetrazolium chloride (TTC) staining 24 h after MCAO (60-min) and neurological deficit score in WT, *Apoe*$^{-/-}$ mice, and *Apoe*$^{-/-}$gM2KO mice (B and C) and in *Trpm2*$^{fl/fl}$ mice, *Apoe*$^{-/-}$*Trpm2*$^{fl/fl}$cre^{-} mice, and *Apoe*$^{-/-}$*Trpm2*$^{fl/fl}$cre^{+} mice (D and E) fed with or without HFD (n = 12–20 mice per group) (scale bar size: 5 mm).

(F and G) TRPM2 expression in brains from WT mice fed with or without HFD (n = 5 and 5 mice).

(H and I) TRPM2 and CD36 expression in primary neurons, CECs, BMDMs, and peripheral leukocytes isolated from WT mice (n = 5, 5, 5, and 5 dishes of cells isolated from at least 5 mice).

(J and K) TRPM2 expression in peripheral leukocytes isolated from WT mice fed with HFD for 0, 1, 2, 3, and 4 months (n = 5, 5, 5, 5, and 5 dishes of cells isolated from at least 5 mice).

(legend continued on next page)

In summary, the data presented earlier demonstrate a significant correlation between TRPM2 expression levels in human peripheral leukocytes and blood lipid levels, as well as systemic inflammation. Given that TRPM2 is a critical driver of immune cell activation,[15] these results suggest that TRPM2 may play an important role in promoting inflammatory responses in the context of hyperlipidemia.

Global TRPM2 knockout abolishes the exacerbation of ischemic brain injury by hyperlipidemia

Given TRPM2's role in ischemic brain injury and its strong correlation with blood lipid levels, we investigated whether TRPM2 upregulation in leukocytes mediates hyperlipidemia's detrimental effects during ischemic stroke. To induce hyperlipidemia, 4- to 5-months-old *Apoe*$^{-/-}$ mice were fed an HFD for at least 4 months. *Apoe*$^{-/-}$ mice develop severe metabolic syndrome following HFD treatment,[13,14] mimicking human stroke pathophysiology. By the time of transient middle cerebral artery occlusion (MCAO) procedure, the mice were 8–10 months old, roughly equivalent to middle-aged humans, making this model highly clinically relevant for stroke in hyperlipidemic individuals.

We observed marked lipid plaque formation in the internal carotid artery in *Apoe*$^{-/-}$ mice induced by HFD, which was not noticeable in global TRPM2 knockout (Figure 2A), highlighting TRPM2's role in atherogenesis.[12] Compared to wild-type (WT) mice, *Apoe*$^{-/-}$ mice exhibited a significantly larger infarct size even without HFD treatment (Figures 2B and 2C and Table S1). HFD treatment further increased the infarct size in *Apoe*$^{-/-}$ mice (Figures 2B and 2C). Global TRPM2 knockout reduced infarct sizes in *Apoe*$^{-/-}$ mice under both control and HFD conditions and prevented HFD-induced exacerbation of infarct size and neurobehavioral impairment (Figures 2B and 2C). Using postnatally induced TRPM2 knockout mice, we confirmed that TRPM2 deletion similarly mitigates infarct size and neurobehavioral deficits in HFD-fed *Apoe*$^{-/-}$ mice (Figures 2D and 2E). These findings underscore TRPM2's critical role in mediating hyperlipidemia's detrimental effects on ischemic brain injury.

We then investigated how TRPM2 influences ischemic brain injury complicated by hyperlipidemia. TRPM2 expression significantly increased in the brain following HFD treatment (Figures 2F and 3G), indicating its involvement in hyperlipidemia-induced brain pathology. To identify the cellular mechanisms, we examined TRPM2 expression in cortical neurons, cerebral endothelial cells (CECs), bone marrow-derived macrophages (BMDMs), and peripheral leukocytes. The results showed that BMDMs and peripheral leukocytes exhibited the highest TRPM2 expression levels, followed by neurons, with CECs having the lowest expression levels (Figures 2H and 2I). Given the close relationship between lipid metabolism and scavenger receptors, particularly CD36, and our previous demonstration of an intriguing regulation between TRPM2 and CD36,[12] we also examined CD36 expression and found that BMDMs and peripheral leukocytes had the highest CD36 expression levels, while cortical neurons showed no detectable CD36 expression (Figures 2H and 2I). These data suggest that TRPM2 in myeloid cells is most likely to mediate the detrimental effects of hyperlipidemia. Thus, we examined TRPM2 expression levels in peripheral leukocytes from *Apoe*$^{-/-}$ mice subjected to HFD treatment and observed a significant increase in TRPM2 expression as early as 2 months after HFD treatment, reaching approximately a 5-fold increase by the end of the 4-month HFD treatment (1.402 ± 0.111 vs. 0.278 ± 0.029) (Figures 2J and 2K).

To identify TRPM2-expressing leukocyte populations, we used ELISA to measure TRPM2 levels in sorted peripheral leukocytes. TRPM2 was primarily expressed in monocytes and neutrophils, with minimal expression in B and T cells (Figure 2L). HFD treatment significantly increased TRPM2 expression in monocytes and neutrophils, indicating that myeloid cells drive hyperlipidemia-induced TRPM2 upregulation in leukocytes (Figure 2L). Additionally, HFD caused a gradual rise in plasma oxLDL and IL-1β levels, which were strongly correlated (Figures 2M–2O). Notably, TRPM2 expression in mouse peripheral leukocytes also strongly correlated with plasma IL-1β and oxLDL levels, consistent with our human data (Figures 2P and 2Q). Collectively, these findings suggest that myeloid cell TRPM2 is likely to mediate the detrimental effects of hyperlipidemia during ischemic stroke.

Increase of TRPM2 expression by hyperlipidemia results in a more pro-inflammatory macrophage phenotype

To explore how hyperlipidemia affects TRPM2 expression in peripheral leukocytes, we hypothesized that LDL induces TRPM2 upregulation, given its strong correlation with TRPM2 expression in humans (Figure 1). First, we examined whether our *in vitro* cell culture conditions lead to any loss of certain peripheral leukocyte population(s). After 24 h in culture, we observed a slight reduction in B cells, leading to a relative increase in T cells, monocytes, and neutrophils (Figures S2G and S2H). Morphological changes in monocytes and neutrophils, likely due to phagocytosis, were noted (Figure S2G), but their proportions remained surprisingly unchanged (Figure S2H). As TRPM2 is predominantly expressed in myeloid cells, this minor B cell loss should not affect our study's conclusions. The average LDL level in our human samples was 76.800 ± 4.747 mg/dL (768 ± 47.47 μg/mL) (Figure 1D). However, LDL treatment at 1,500 μg/mL (150 mg/dL) did not significantly increase TRPM2 expression in isolated human leukocytes, even after 48 h (Figures 3A and 3B).

We shifted focus to oxLDL, hypothesizing that oxLDL induces TRPM2 upregulation, as LDL readily transforms into oxLDL *in vivo*.[21] The average oxLDL level in our human blood samples

(L) ELISA measurement of TRPM2 levels in lysates from B cells, T cells, monocytes, and neutrophils after cell sorting of peripheral leukocytes from WT mice with or without HFD treatment.
(M and N) ELISA measurement of plasma oxLDL and IL-1β levels in WT mice fed with HFD for 0, 1, 2, 3, and 4 months (n = 5, 5, 5, 5, and 5 plasma samples from different mice).
(O and P) Correlation of plasma IL-1β level with plasma oxLDL level (O) and TRPM2 expression (P) in peripheral leukocytes (n = 5 mice).
(Q) Correlation of plasma oxLDL level with TRPM2 expression in peripheral leukocytes (n = 5 mice).
Error bars: mean ± SEM; ns, no statistical significance, *, $p < 0.05$, **, $p < 0.01$, ***, $p < 0.001$. See also Figure S2 and Table S1.

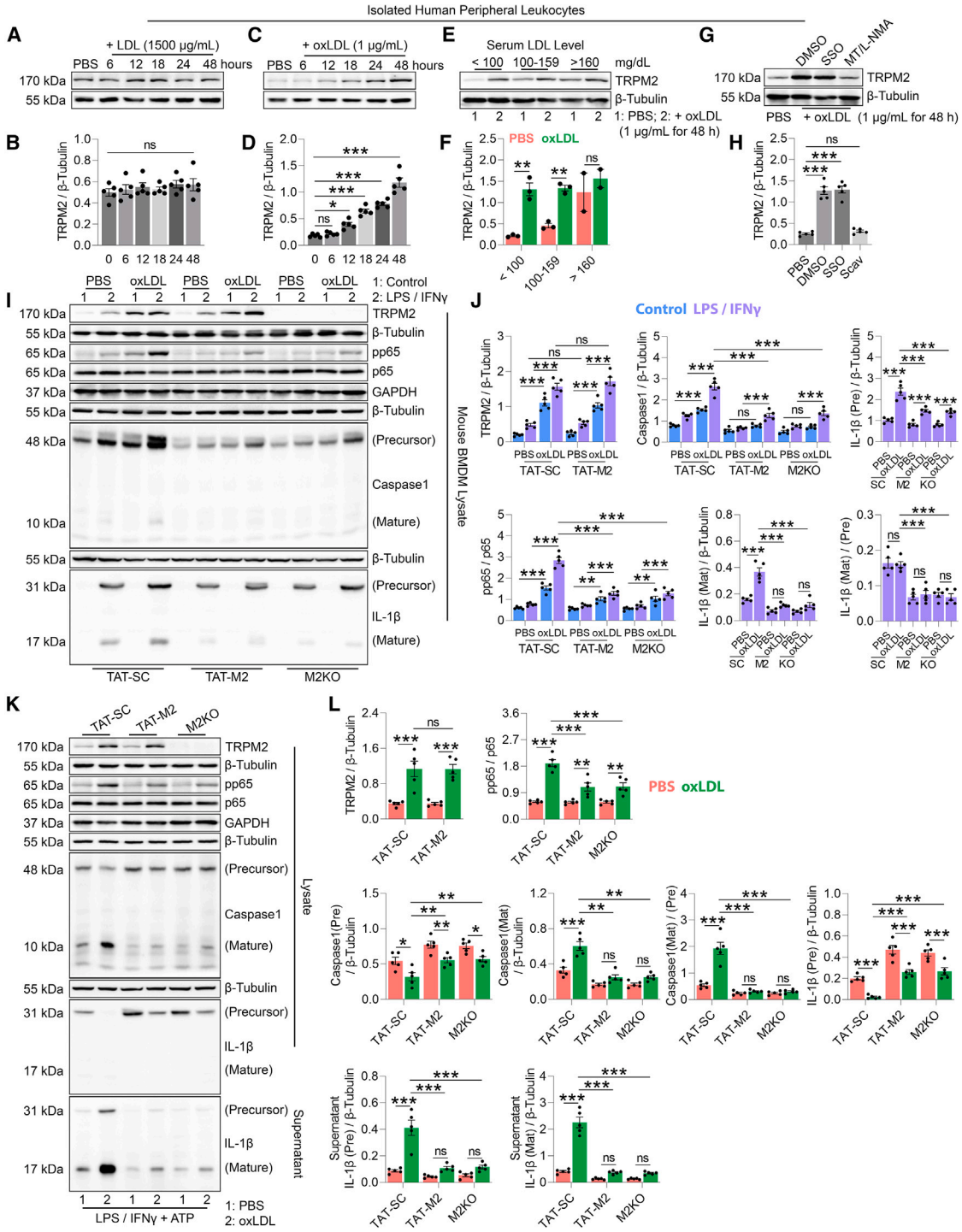

Figure 3. Increase of TRPM2 expression by hyperlipidemia generates a pro-inflammatory macrophage phenotype

(A–D) TRPM2 expression in human peripheral leukocytes treated with LDL (A and B) and oxLDL (C and D) for 0, 6, 12, 18, 24, and 48 h (n = 5 human individuals).

(E and F) TRPM2 expression in human peripheral leukocytes treated with oxLDL for 48 h (n = 3, 3, and 2 human individuals).

(G and H) TRPM2 expression in WT mouse peripheral leukocytes treated with oxLDL for 48 h with the co-treatment of DMSO, SSO, and scavengers Mn (III) TBAP and L-NMA (n = 5 dishes of cells isolated from at least 5 mice).

(legend continued on next page)

was 38.840 ± 2.590 μg/dL (388.4 ± 25.9 ng/mL) (Figure 1I). We chose to use oxLDL at 1,000 ng/mL (100 μg/dL) for treatment to mimic physiological conditions, although this concentration is relatively low for *in vitro* treatment (usually 50 to 100 μg/mL).[22] Notably, oxLDL treatment at 1 μg/mL (1,000 ng/mL) significantly induced TRPM2 expression in human peripheral leukocytes as early as 12 h after treatment, reaching a more than 6-fold increase by the end of the 48-h HFD treatment (1.182 ± 0.188 vs. 0.184 ± 0.014) (Figures 3C and 3D). Interestingly, peripheral leukocytes isolated from individuals with high LDL levels appeared to have smaller folds of increase (Figures 3E and 3F), likely due to elevated baseline TRPM2. The CD36 inhibitor sulfo-N-succinimidyl oleate (SSO) did not block TRPM2 upregulation, suggesting that other scavenger receptors or membrane signaling via lectin-like oxidized low-density lipoprotein receptor-1 (LOX-1) may mediate oxLDL uptake (Figures 3G and 3H).[23] In contrast, co-incubation with oxidative stress scavengers Mn(III)tetrakis(4-benzoic acid)porphyrin Chloride (Mn (III) TBAP) (1 μM) and NG-Methyl-L-arginine (L-NMA) (1 μM) completely inhibited TRPM2 upregulation, indicating that oxLDL induces TRPM2 expression via oxidative stress. Thus, oxLDL, not LDL, drives TRPM2 upregulation in leukocytes during hyperlipidemia.

To extend our findings, we investigated oxLDL's effects on TRPM2 expression in mouse BMDMs, which offer greater accessibility than human blood samples. Treatment with 1 μg/mL oxLDL induced TRPM2 expression in BMDMs, peaking within 24 h, faster than in human leukocytes (Figures S2I and S2J). This was accompanied by gradual nuclear factor κB (NF-κB) activation, evidenced by elevated pp65 levels (Figures S2I and S2J). LDL (1500 μg/mL) did not induce TRPM2 expression in BMDMs (Figures S2K upper part and S2L), and oxLDL did not increase CD36 expression at 1 μg/mL (Figures S2K lower part and S2L), consistent with higher oxLDL thresholds typically required for CD36 induction. Moreover, the induction of TRPM2 expression and NF-κB activation was inhibited by scavengers, but not by SSO (Figures S2M and S2N). Furthermore, we explored the role of NF-κB signaling in inducing TRPM2 expression using SN50, which inhibits the nuclear translocation of the NF-κB complex.[24] The results showed that SN50 at 100 μg/mL inhibited the induction of TRPM2 expression by oxLDL, suggesting that NF-κB signaling contributes to this process (Figures S2O and S2P). Interestingly, TRPM2 knockout reduced p65 phosphorylation, suggesting that TRPM2 enhances NF-κB signaling (Figures S2O and S2P). These findings demonstrate that oxLDL induces TRPM2 upregulation via oxidative stress and NF-κB signaling.

After identifying how hyperlipidemia induces TRPM2 expression, we investigated its functional consequences. We examined the responses of BMDMs to LPS/interferon γ (IFNγ) priming and ATP stimulation.[25] oxLDL preincubation significantly enhanced pp65, caspase-1, and IL-1β levels after LPS/IFNγ priming, an effect inhibited by the specific TRPM2 inhibitor, TAT-M2 (TAT-M2NX),[26] and TRPM2 knockout (Figures 3I and 3J). Similarly, oxLDL-enhanced ATP-stimulated IL-1β release was blocked by TAT-M2 and TRPM2 knockout (Figures 3K and 3L). These findings indicate that TRPM2 upregulation by oxLDL "primes" BMDMs, promoteing their pro-inflammatory activation, driving a more aggressive phenotype, which may underlie the reduced hyperlipidemia-exacerbated ischemic injury observed in *Apoe*$^{-/-}$ mice with global TRPM2 knockout.

Myeloid cell-specific TRPM2 knockout abolishes the exacerbation of ischemic brain injury by hyperlipidemia

To investigate the role of TRPM2 activity in hyperlipidemia-induced BMDM activation in a stroke model, we generated myeloid cell-specific TRPM2 knockout mice by crossing *Cd11b-cre* mice with *Apoe*$^{-/-}$ mice (Figure 4A). Even in the control group, *Trpm2*$^{fl/fl}$*Cd11b-cre*$^{+}$ mice exhibited a reduced infarct size and preserved neurobehavioral performance compared to *Trpm2*$^{fl/fl}$*Cd11b-cre*$^{-}$ mice (Figures 4A and 4B and Table S1). While previous studies using bone marrow transplantation demonstrated TRPM2's role in peripheral immune cells,[27] our findings confirm that TRPM2 in myeloid cells exacerbates ischemic brain injury using solid knockout models. Moreover, myeloid cell-specific TRPM2 knockout not only reduced the infarct size and compromise of neurobehavior performance in *Apoe*$^{-/-}$ mice in both control and HFD groups but also completely abolished the HFD-induced exacerbation (Figures 4A and 4B). Meanwhile, we found that myeloid cell-specific TRPM2 knockout did not influence mouse body weight (Figure 4C).

To confirm that myeloid cell-specific TRPM2 knockout attenuates immune cell invasion in the brain, we performed flow cytometry after a 24-h reperfusion following a 60-min MCAO (Figure S3A). In controls, TRPM2 knockout significantly reduced immune cell invasion in the ipsilateral hemisphere (MCAO side) of *Apoe*$^{-/-}$ mice but had no effect on lymphocytes (T cells and natural killer [NK] cells) (Figures 4D, 4E, 4H, and 4I), suggesting that TRPM2 is not essential for lymphocyte activation, consistent with a recent report.[28] Conversely, myeloid cell infiltration, including neutrophils and monocytes/macrophages, was markedly reduced (Figures 4D, 4E, 4J, and 4K). Microglial proliferation and activation (Ly6C) remained unchanged, likely due to their delayed peak activation post-stroke (Figures 4D, 4E, and 4L).[29] HFD treatment greatly increased immune cell invasion, worsening ischemic brain injury, but TRPM2 knockout inhibited leukocyte, neutrophil, and monocyte/macrophage infiltration under HFD conditions, without affecting lymphocytes (Figures 4F, 4G, and 4H–4L). Interestingly, HFD also increased T cell infiltration, likely due to passive BBB leakage (Figures 4D, 4F, and 4H–4L), and unexpectedly enhanced immune cell invasion in the contralateral hemisphere (non-MCAO side) (Figures S3B, S3D, and S3F–S3J), suggesting systemic hyperlipidemia effects, which were also inhibited by TRPM2 knockout (Figures S3B–S3J). Peripheral blood

(I and J) TRPM2, pp65, caspase-1, and IL-1β (precursor and mature) expression in WT and M2KO mouse BMDMs primed with LPS and IFNγ for overnight, with or without the preincubation of oxLDL for 48 h (n = 5 dishes of cells isolated from at least 5 mice).
(K and L) Examination of macrophage IL-1β release (n = 5 dishes of cells isolated from at least 5 mice). Proteins in supernatant were isolated using trichloroacetic acid (TCA) precipitation.
Error bars: mean ± SEM; ns, no statistical significance, *, $p < 0.05$, **, $p < 0.01$, ***, $p < 0.001$. See also Figure S2.

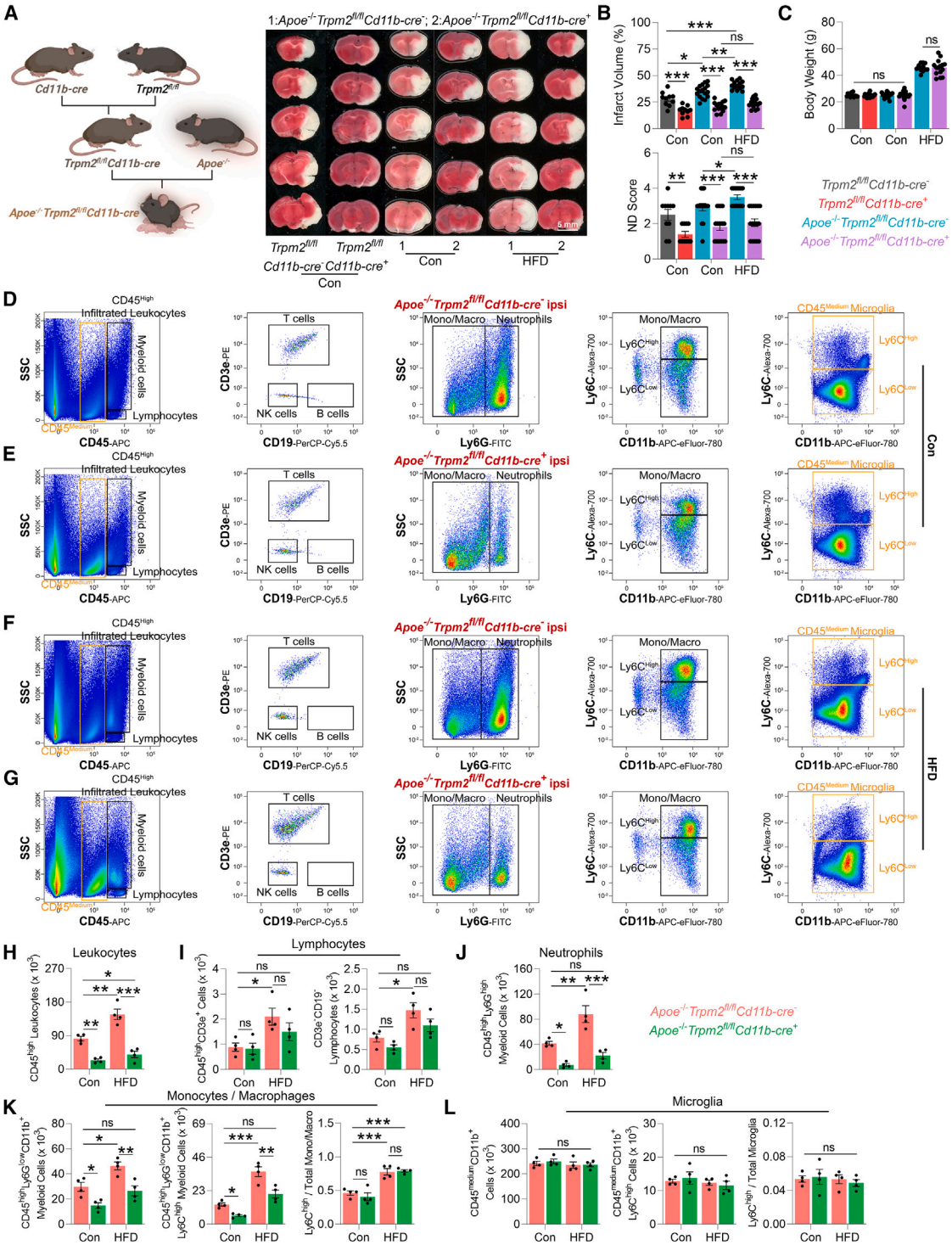

Figure 4. Myeloid cell-specific TRPM2 knockout abolishes the exacerbation of ischemic brain injury by hyperlipidemia

(A and B) TTC staining 24 h after MCAO (60-min) and neurological deficit score in *Trpm2*$^{fl/fl}$*Cd11b-cre*$^{-}$ mice, *Trpm2*$^{fl/fl}$*Cd11b-cre*$^{+}$ mice, *Apoe*$^{-/-}$*Trpm2*$^{fl/fl}$ *Cd11b-cre*$^{-}$ mice, and *Apoe*$^{-/-}$*Trpm2*$^{fl/fl}$*Cd11b-cre*$^{+}$ mice fed with or without HFD (n = 12–20 mice per group) (scale bar size: 5 mm).

(C) Quantification of body weight of the mice used.

(D–G) Flow cytometry analysis of the post-MCAO immune cell infiltration and microglia activation in the ipsilateral (right) hemisphere of *Apoe*$^{-/-}$*Trpm2*$^{fl/fl}$*Cd11b-cre*$^{-}$ mice and *Apoe*$^{-/-}$*Trpm2*$^{fl/fl}$*Cd11b-cre*$^{+}$ mice fed with or without HFD.

(H–L) Quantification of total leukocytes (H), lymphocytes (I), neutrophils (J), monocytes/macrophages (K), and microglia (L) counts (n = 4 mice per group).

Error bars: mean ± SEM; ns, no statistical significance, *, $p < 0.05$, **, $p < 0.01$, ***, $p < 0.001$. See also Figures S3 and S4 and Table S1.

analysis confirmed no changes in leukocyte populations, ruling out compromised hematopoiesis (Figures S4A–S4H). These findings highlight that hyperlipidemia-induced TRPM2 expression in myeloid cells drives immune cell invasion, exacerbating ischemic brain injury.

The increase of TRPM2 expression by oxLDL compromises the resistance of endothelial cells to ischemia

As endothelial function is compromised during hyperlipidemia,[30,31] and endothelial hyperpermeability markedly exacerbates ischemic brain injury,[32,33] we further examined the potential contribution of TRPM2 in endothelial dysfunction induced by the physiologically reachable concentration of oxLDL. Despite exhibiting low baseline TRPM2 expression level, CECs showed a significant increase in TRPM2 expression as early as 12 h after treatment with oxLDL at 1 μg/mL, accompanied by an increase in pp65 levels (Figures 5A and 5B). Similar to BMDMs, treatment with LDL at 1,500 μg/mL failed to induce TRPM2 expression (Figures 5C and 5E), and oxLDL treatment did not alter CD36 expression (Figures 5D and 5F). The upregulation of TRPM2 expression and activation of NF-κB signaling were not influenced by the CD36 inhibitor SSO but were abolished by co-incubation with scavengers (Figures 5G and 5H). These results suggest that TRPM2 may play a role in hyperlipidemia-induced endothelial dysfunction.

We next examined the consequences of upregulated TRPM2 expression in CECs. OxLDL had no effect on occludin (tight junction marker) or caspase-3 (apoptosis marker) expression (Figures S4I and S4J) but significantly increased nitric oxide synthase (iNOS) expression, indicating elevated oxidative stress in CECs.[34] The oxLDL-induced iNOS increase was inhibited by the NF-κB nuclear translocation inhibitor SN50, TRPM2 inhibitors (ACA and TAT-M2), and TRPM2 knockout (Figures 5I and 5J). TRPM2 inhibition/knockout also suppressed pp65 phosphorylation, suggesting that oxLDL induces iNOS via TRPM2-dependent NF-κB activation (Figures 5I and 5J). We then tested whether oxLDL-induced oxidative stress in CECs affects ischemic responses. While oxLDL alone did not alter occludin expression, its preincubation significantly accelerated occludin degradation under oxygen-glucose deprivation (OGD) (Figures 5K and 5L). This may be linked to enhanced oxidative stress, as oxLDL preincubation further increased iNOS expression post-OGD (Figures 5K and 5L). Notably, TAT-M2 and TRPM2 knockout inhibited both accelerated occludin degradation and iNOS upregulation (Figures 5K and 5L). Similarly, oxLDL preincubation significantly accelerated barrier function loss in CECs, affecting ion transfer across transwell inserts (Figures 5M and 5N) and increasing permeability to larger molecules like Evans blue (Figure 5O). Both effects were effectively blocked by TAT-M2 and TRPM2 knockout. These results suggest that similar to macrophages, oxLDL-induced TRPM2 upregulation "primes" CECs and drives oxidative stress, thereby decreasing their resistance to ischemia.

Endothelial cell-specific TRPM2 knockout abolishes the exacerbation of ischemic brain injury by hyperlipidemia

Building on TRPM2's role in hyperlipidemia-induced CEC dysfunction, we examined its impact in a stroke model. Using *Cdh5-cre* mice crossed with *Apoe*$^{-/-}$ mice to create a hyperlipidemia model, we achieved endothelial-specific TRPM2 knockout (Figure 6A). Consistent with our previous report, *Trpm2*$^{fl/fl}$*Cdh5-cre*$^{+}$ mice showed reduced infarct size and preserved neurobehavioral performance compared to *Trpm2*$^{fl/fl}$*Cdh5-cre*$^{-}$ mice (Figures 6A and 6B and Table S1). The exciting finding here was that endothelial-specific TRPM2 knockout also reduced the infarct size and worsening of neurobehavior performance in *Apoe*$^{-/-}$ mice in both control and HFD groups and completely abolished the further increase in infarct size and worsening of neurobehavior performance induced by HFD treatment (Figures 6A and 6B). Meanwhile, endothelial-specific TRPM2 knockout did not influence the body weight of mice (Figure 6C). Compromised endothelial function leads to reduced local micro-perfusion after stroke,[35] and our *in vivo* cerebral perfusion analysis revealed that HFD further reduced brain perfusion in the ipsilateral MCA territory after MCAO in *Apoe*$^{-/-}$ mice, a detrimental effect prevented by TRPM2 knockout (Figures 6D and 6E). These results highlight endothelial-specific TRPM2 knockout's benefit in preserving micro-perfusion and mitigating hyperlipidemia-induced ischemic damage.

Hyperlipidemia and HFD treatment impair BBB structure and function, causing lipid accumulation in brain arterioles,[36] reduced tight junction molecule expression, and increased permeability.[37] We investigated whether endothelial-specific TRPM2 knockout could mitigate BBB integrity loss after stroke in hyperlipidemic mice. To assess BBB leakage and plasma extravasation, we used the Evans blue assay, measuring fluorescence intensity (excitation: 620 nm, emission: 680 nm), a sensitive and accurate method for quantifying leakage[38] and evaluating vascular permeability.[39,40] In *Apoe*$^{-/-}$*Trpm2*$^{fl/fl}$*Cdh5-cre*$^{-}$ mice, HFD treatment caused a massive increase in Evans blue leakage (relative to the contralateral hemisphere), with extensive staining of damaged cortical neurons. In contrast, *Apoe*$^{-/-}$*Trpm2*$^{fl/fl}$*Cdh5-cre*$^{+}$ mice were resistant to post-stroke Evans blue leakage, and HFD did not exacerbate leakage (Figures 6F–6H). To avoid bias from immunofluorescence intensity comparisons, we measured absolute Evans blue absorbance in brain lysates, confirming reduced leakage in *Trpm2*$^{fl/fl}$*Cdh5-cre*$^{+}$ mice and prevention of HFD-induced exacerbation (Figure 6I). Moreover, HFD also increased leakage into the contralateral hemisphere, indicating systemic BBB damage under hyperlipidemia, which was absent in *Trpm2*$^{fl/fl}$*Cdh5-cre*$^{+}$ mice (Figure 6I).

To assess the effects of endothelial TRPM2 knockout on BBB morphology post-stroke, we examined structural changes following MCAO. Ischemia reduced capillary density (Figure 6J), length (Figure S5A), and branching (Figure S5B), while increasing tortuosity (Figure S5C), indicating BBB damage, all of which were exacerbated by HFD (Figures 6J and S5A–S5C).[41] In contrast, these ischemia-induced changes were all attenuated in *Trpm2*$^{fl/fl}$*Cdh5-cre*$^{+}$ mice, with no additional effects from HFD (Figures 6J and S5A–S5C). Interestingly, while HFD increased BBB functional leakage in the contralateral hemisphere (Figure 6I), no significant morphological changes were observed there (Figures 6J and S5A–S5C). This aligns with *in vitro* findings showing that TRPM2 increases endothelial susceptibility to ischemia under hyperlipidemia but does not affect basal barrier function. These results underscore endothelial

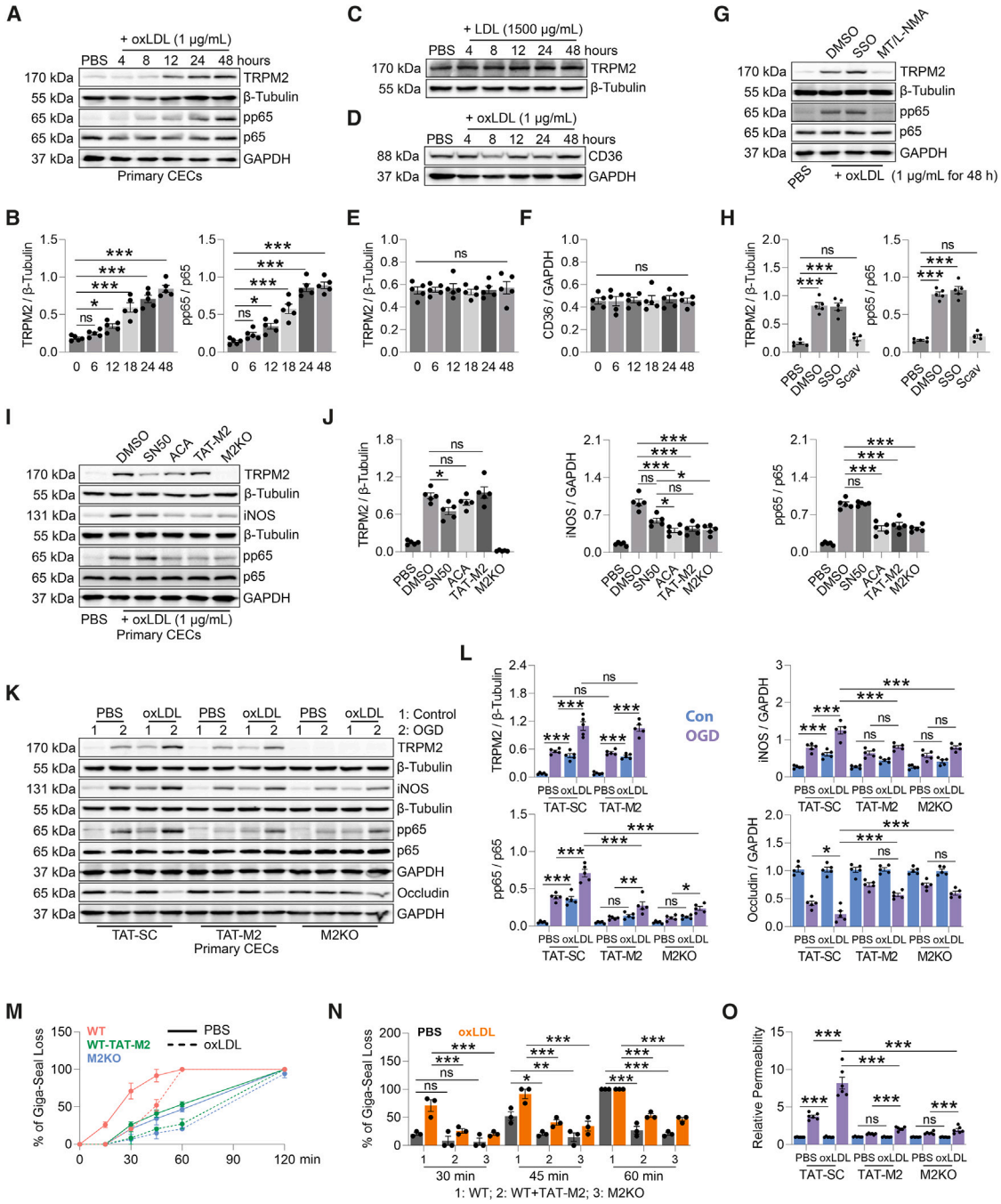

Figure 5. Increase of TRPM2 expression by oxLDL compromises resistance of endothelial cells to ischemia

(A–C and E) TRPM2 and pp65 expression in primary CECs isolated from WT mouse treated with oxLDL (A and B) and LDL (C and E) for 0, 6, 12, 18, 24, and 48 h ($n = 5$).

(D and F) CD36 expression in primary CECs isolated from WT mouse treated with oxLDL for 0, 6, 12, 18, 24, and 48 h ($n = 5$).

(G and H) TRPM2 expression in WT mouse primary CECs treated with oxLDL for 48 h with the co-treatment of DMSO, SSO, and scavengers Mn (III) TBAP and L-NMA ($n = 5$).

(I and J) TRPM2, iNOS, and pp65 expression in WT and M2KO mouse primary CECs treated with oxLDL for 48 h with the co-treatment of DMSO, SN50, ACA, and TAT-M2 ($n = 5$).

(K and L) Examination of endothelial responses to *in vitro* ischemia insult. TRPM2, iNOS, pp65, and occludin expression in WT and M2KO mouse primary CECs subjected to OGD for 8 h ($n = 5$).

(M and N) Monitoring of the loss of giga-seal after OGD in transwell inserts plated with WT or M2KO mouse primary CECs pretreated with oxLDL for 48 h ($n = 3$).

(O) Measurement of the leakage of Evans blue (related to the PBS-Con groups) from upper into lower chamber 8 h after OGD in transwell inserts ($n = 6$).

n means X dishes of cells isolated from at least X mice per group; error bars: mean ± SEM; ns, no statistical significance, *, $p < 0.05$, **, $p < 0.01$, ***, $p < 0.001$.

CellPress
OPEN ACCESS

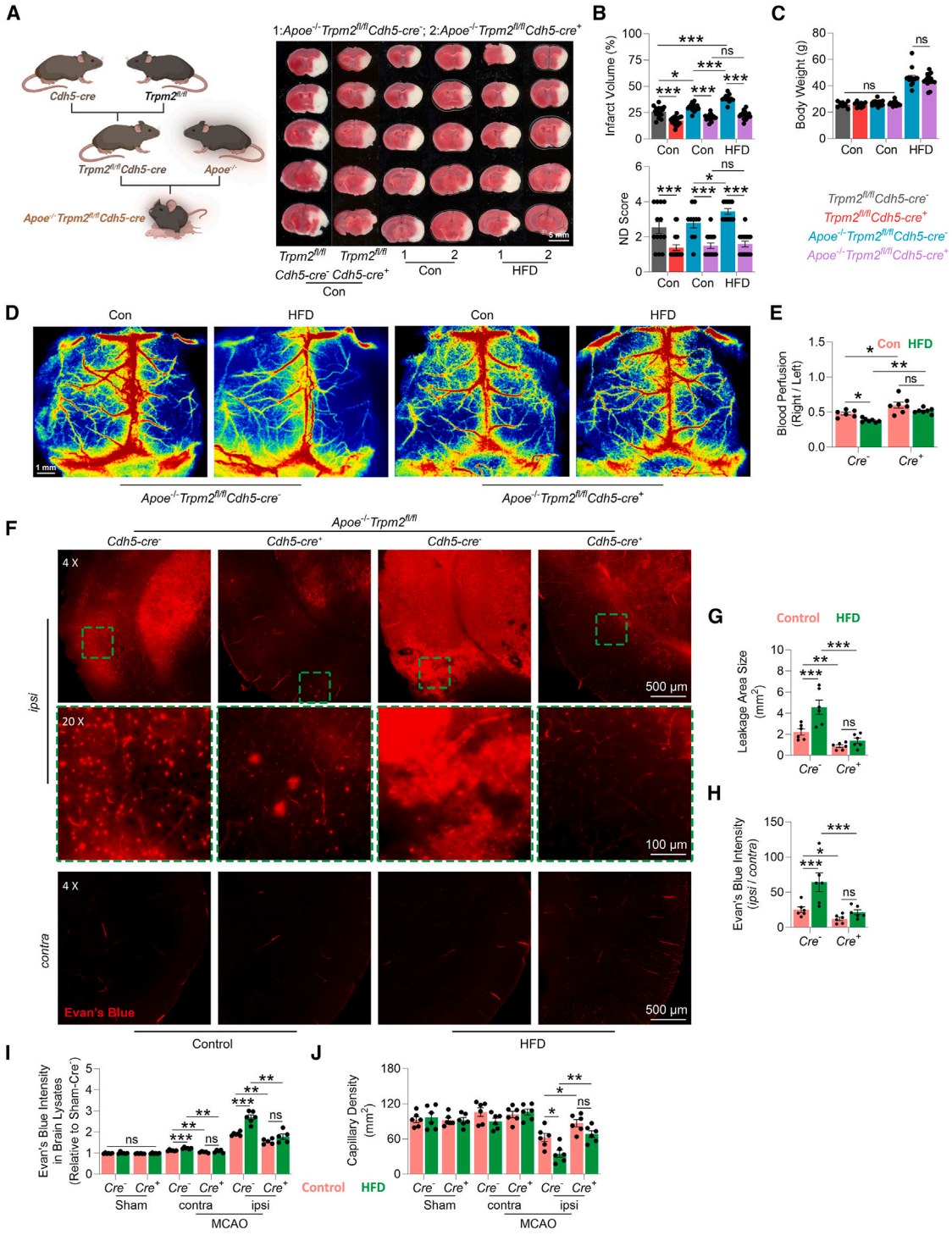

Figure 6. Endothelial-specific TRPM2 knockout abolishes the exacerbation of ischemic brain injury by hyperlipidemia

(A and B) TTC staining 24 h after MCAO (60-min) and neurological deficit score in *Trpm2*$^{fl/fl}$*Cdh5-cre*$^{-}$ mice, *Trpm2*$^{fl/fl}$*Cdh5-cre*$^{+}$ mice, *Apoe*$^{-/-}$*Trpm2*$^{fl/fl}$*Cdh5-cre*$^{-}$ mice, and *Apoe*$^{-/-}$*Trpm2*$^{fl/fl}$*Cdh5-cre*$^{+}$ mice fed with or without HFD (n = 12–20 mice per group) (scale bar size: 5 mm).

(C) Quantification of body weight of the mice used.

(D and E) Blood flow image showing cerebral perfusion after MCAO in *Apoe*$^{-/-}$*Trpm2*$^{fl/fl}$*Cdh5-cre*$^{-}$ mice and *Apoe*$^{-/-}$*Trpm2*$^{fl/fl}$*Cdh5-cre*$^{+}$ mice fed with or without HFD (n = 6, 7, 7, and 7 mice) (scale bar size: 1 mm).

(F–H) Representative images of Evans blue leakage (F) into the brain in both left (*contralateral*, 4X) and right (*ipsilateral*, 4X and 20X [green rectangular area under 4X]) hemisphere from *Apoe*$^{-/-}$*Trpm2*$^{fl/fl}$*Cdh5-cre*$^{-}$ mice and *Apoe*$^{-/-}$*Trpm2*$^{fl/fl}$*Cdh5-cre*$^{+}$ mice fed with or without HFD after MCAO model (scale bar size: 100 μm

(legend continued on next page)

TRPM2's critical role in mediating hyperlipidemia's detrimental effects on BBB function.

We then examined BBB permeability to immune cell infiltration and found that endothelial-specific TRPM2 knockout, similar to myeloid-specific TRPM2 knockout, inhibited total leukocyte infiltration in the ipsilateral hemisphere of *Apoe*$^{-/-}$ mice in the control group (Figures S5D, S5E, and S5H). However, lymphocyte infiltration (T cells and NK cells) was unaffected, likely due to their minimal involvement in early ischemic stroke (Figures S5D, S5E, and S5I). In contrast, myeloid cell infiltration, including neutrophils and monocytes/macrophages, was significantly reduced (Figures S5D, S5E, S5J, and S5K). Despite reduced brain injury, microglial activation (Ly6C) showed no significant differences (Figures S5D, S5E, and S5L). HFD treatment significantly increased the invasion of all immune cell populations, exacerbating ischemic brain injury (Figures S5D, S5F, and S5H–S5L). Endothelial-specific TRPM2 knockout in HFD groups effectively inhibited the infiltration of total leukocytes, neutrophils, and monocytes/macrophages in the ipsilateral hemisphere but did not affect T cell or NK cell infiltration (Figures S5F, S5G, and S5H–S5L). Additionally, HFD enhanced immune cell invasion in the contralateral hemisphere, indicating hyperlipidemia's systemic detrimental effects on BBB. This increase was also mitigated by endothelial-specific TRPM2 knockout (Figures S6A–S6I). Peripheral blood analysis showed no changes in immune cell distribution, ruling out compromised hematopoiesis (Figure S7). These findings suggest that hyperlipidemia-induced TRPM2 expression in endothelial cells promotes BBB leakage and exacerbates ischemic brain injury.

Increase of TRPM2 expression by oxLDL compromises resistance of neurons to ischemia

Previous studies have demonstrated the direct neurotoxic effects of oxLDL.[42] We found substantially increased oxLDL infiltration in the ipsilateral hemisphere of HFD-fed *Apoe*$^{-/-}$ mice (Figure 7A). In primary cortical neurons, oxLDL (1 μg/mL) rapidly upregulated TRPM2 expression, accompanied by an increase in pp65 levels, suggesting the activation of NF-κB signaling (Figures 7B and 7C). Unlike CECs, oxLDL increased cleaved caspase-3 expression in neurons (Figures 7B and 7C), suggesting the induction of apoptosis. In contrast, LDL (1,500 μg/mL) failed to induce TRPM2 expression or apoptosis (Figures 7D and 7E). Similar to BMDMs and CECs, the increase in TRPM2 and pp65 levels was abolished by scavengers (Figures 7F and 7G), suggesting that these changes were caused by the oxidative stress induced by oxLDL. Considering that TRPM2 directly enhances glutamate excitotoxicity,[43] we further examined the role of excitotoxicity in oxLDL-induced neuronal death. However, oxLDL-induced neurotoxicity was independent of glutamate excitotoxicity, as NMDA receptor blockers MK801 and AP5 had no protective effect (Figures 7H and 7I). In contrast, NF-κB inhibitor SN50, TRPM2 inhibitor TAT-M2, and TRPM2 knockout suppressed oxLDL-induced apoptosis and pp65 upregulation (Figures 7H and 7I). These findings suggest that TRPM2 mediates oxLDL-induced NF-κB activation and neuronal apoptosis, directly contributing to hyperlipidemia's neurotoxic effects during ischemic stroke.

TRPM2-specific inhibitor abolishes the exacerbation of ischemic brain injury by hyperlipidemia

Finally, we assessed the translational significance of our findings by examining the protective effects of the TRPM2 inhibitor in a 7-day long-term stroke model. TAT-SC (scramble) or TAT-M2 was administered intraperitoneally (10 nmol/kg, daily) after the MCAO procedure (Figure 7J, right). We observed that TAT-M2 abolished the enhanced infarct size caused by HFD treatment, accompanied by the preservation of neurological deficit scores and performance in the rotarod assay, without influencing the body weight of *Apoe*$^{-/-}$ mice (Figures 7J–7L). These results suggest that TRPM2 is a promising therapeutic target for attenuating the exacerbation of ischemic brain injury by hyperlipidemia.

DISCUSSION

Previous studies have established a strong link between plasma LDL levels and cardiovascular risks,[44] with lipid-lowering therapy improving neurological outcomes in stroke patients.[5] Our study revealed a stronger correlation between plasma oxLDL levels and the systemic inflammation marker IL-1β compared to LDL. Moreover, *in vitro* experiments showed that oxLDL, but not LDL, drives hyperlipidemia-induced cellular dysfunction. These findings suggest that oxLDL may be a more precise and reliable biomarker for assessing cardiovascular risks than LDL. TRPM2 is an important contributor to the activation of myeloid cells, and increased monocyte activation is observed in individuals with hyperlipidemia.[16,17] However, its correlation with plasma lipid levels had not been explored. Here, we identified a strong correlation between TRPM2 expression in peripheral leukocytes and plasma lipid levels in humans. Notably, TRPM2 expression correlated more strongly with IL-1β, a systemic inflammation marker, than with LDL or oxLDL. Given the associations of LDL, oxLDL, and IL-1β with major adverse cardiovascular events,[44–46] our findings highlight TRPM2 expression in leukocytes as a promising predictor of cardiovascular risks.

Although TRPM2's role in exacerbating ischemic stroke is well-documented,[26,27,33,43,47,48] previous studies relied on mouse models with limited clinical relevance.[7] In contrast, *Apoe*$^{-/-}$ mice fed with HFD typically develop comorbidities commonly seen in human stroke patients, including hyperlipidemia, hypertension, obesity, and insulin resistance.[13,14] Using conditional knockouts, we demonstrated that hyperlipidemia-induced TRPM2 overactivity in myeloid and endothelial cells aggravates inflammation and BBB leakage, worsening ischemic

for 20× magnification and 500 μm for 40× magnification). Quantification of the size of Evans blue leakage area (G) and the relative Evans blue intensity in the MCAO side compared to the contralateral side (H) (n = 6 mice per group).

(I and J) Quantification of Evans Blue intensity in brain lysates (relative to the sham groups) (I) and capillary density (J) in the right hemisphere of sham groups and both left and right hemisphere of MCAO groups from *Apoe*$^{-/-}$*Trpm2*$^{fl/fl}$*Cdh5-cre*$^{-}$ mice and *Apoe*$^{-/-}$*Trpm2*$^{fl/fl}$*Cdh5-cre*$^{+}$ mice fed with or without HFD (n = 6 mice per group).

Error bars: mean ± SEM; ns, no statistical significance, *, $p < 0.05$, **, $p < 0.01$, ***, $p < 0.001$. See also Figures S5, S6, and S7 and Table S1.

CellPress
OPEN ACCESS

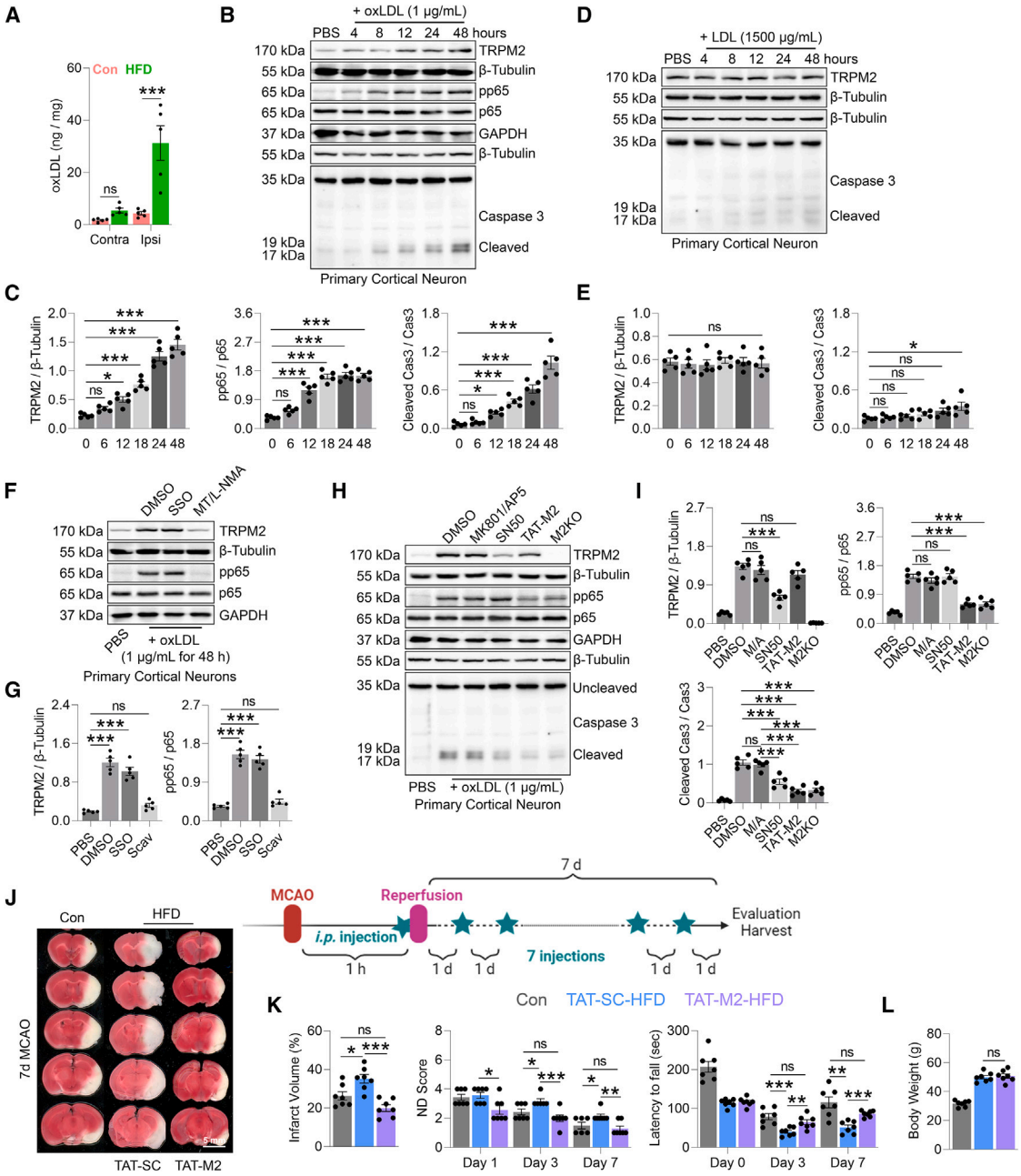

Figure 7. Increase of TRPM2 expression by oxLDL compromises resistance of neurons to ischemia

(A) ELISA measurement of oxLDL amount in the brain tissue of the contralateral (left) and ipsilateral (right) hemisphere 24 h after MCAO.

(B–E) TRPM2, pp65, and caspase-3 expression in primary cortical neurons isolated from WT mouse treated with oxLDL (B and C) and LDL (D and E) for 0, 6, 12, 18, 24, and 48 h (n = 5 dishes of cells isolated from at least 5 mice).

(F and G) TRPM2 expression in WT mouse primary cortical neurons treated with oxLDL for 48 h with the co-treatment of DMSO, SSO, and scavengers Mn (III) TBAP and L-NMA (n = 5 dishes of cells isolated from at least 5 mice).

(H and I) TRPM2, pp65, and caspase-3 expression in WT and M2KO mouse primary cortical neurons treated with oxLDL for 48 h with the co-treatment of DMSO, MK801/AP5, SN50, ACA, and TAT-M2 (n = 5 dishes of cells isolated from at least 5 mice).

(J and K) Graphic illustration of the administration strategy, as well as quantification and representative images of TTC staining 7 days after MCAO, neurological deficit score, and rotarod performance in *Apoe*$^{-/-}$ mice fed with or without HFD. TAT-SC and TAT-M2 were injected intraperitoneally (10 nmol/kg) right after reopening of MCA (n = 7, 7, and 7 mice) (scale bar size: 5 mm).

(L) Quantification of body weight of the mice used.

Error bars: mean ± SEM; ns, no statistical significance, *, $p < 0.05$, **, $p < 0.01$, ***, $p < 0.001$.

brain injury. These findings underscore the translational potential of TRPM2 inhibition for ischemic stroke.

Lipid deposition in brain vasculature during hyperlipidemia is well-documented, but whether lipid leakage into the parenchyma contributes to ischemic brain injury remains unclear.[36] Circulating oxLDL level, which predicts prognosis, is elevated in stroke patients; however, its specific role in ischemic injury is poorly understood.[46,49] We observed substantially higher oxLDL concentrations in the ischemic hemisphere of HFD-treated mice. Given oxLDL's excitotoxicity-independent neurotoxicity at low concentrations, our findings suggest that leaked oxLDL directly contributes to ischemic brain injury. Notably, TRPM2 inhibition and knockout mitigated oxLDL-induced neuronal death, highlighting the therapeutic potential of targeting TRPM2 to reduce lipid-driven neurotoxicity in ischemic stroke.

In summary, we demonstrate that TRPM2 plays a pivotal role in mediating the detrimental effects of hyperlipidemia on ischemic brain injury in middle-aged *Apoe*$^{-/-}$ mice, a model that closely mimics human stroke pathophysiology. Our findings highlight TRPM2 as a promising therapeutic target for hyperlipidemia-exacerbated ischemic injury and suggest its potential as a peripheral blood biomarker for stroke outcomes.

Limitations of the study

Firstly, the limited number of participants with severe hyperlipidemia, likely due to effective lipid management, constrains the generalizability of our findings. Future investigation with a large number of participants is needed to better assess the roles of oxLDL and TRPM2 in systemic inflammation and cardiovascular risks. Secondly, determining the specific contribution of myeloid cell activation to BBB integrity under HFD and post-stroke conditions remains challenging, as, under *in vivo* conditions, it is difficult to distinguish between the direct effects on the BBB during myeloid cell adhesion and migration through the BBB and the indirect effects once myeloid cells enter the parenchyma and initiate inflammatory responses. Future comprehensive evaluations using chimeric mice will be necessary to determine whether endothelial TRPM2 or immune TRPM2 plays a more significant role in causing BBB damage during ischemic stroke and under hyperlipidemic conditions. Lastly, this study was conducted exclusively in male mice. Future investigations incorporating female mice will be necessary for a more comprehensive evaluation of potential sex-specific differences in TRPM2-mediated BBB dysfunction and stroke pathogenesis.

RESOURCE AVAILABILITY

Lead contact

Further information and requests for resources and reagents should be directed to and will be fulfilled by the lead contact Lixia Yue (lyue@uchc.edu).

Materials availability

All unique/stable reagents and mouse strains generated in this study are available from the lead contact with a completed Materials and Animal Transfer Agreement.

Data and code availability

- All original data will be available upon contacting Lixia Yue (lyue@uchc.edu).
- This paper does not report original code.
- Any additional information required to reanalyze the data reported in this work paper is available from the lead contact upon request.

ACKNOWLEDGMENTS

We thank Louise McCullough (UTHealth) for insightful discussions and Dr. Andrew M. Scharenberg (University of Washington) for providing the TRPM2 plasmid. This work was supported in part by NIH grants R01-HL171486 and R01-NS131661 and AHA grant 19TPA34890022 to L.Y., as well as a Connecticut Institute for the Brain and Cognitive Sciences Seed Grant (402194) to P.Z.

AUTHOR CONTRIBUTIONS

L.Y. and P.Z. conceived the project. B.L. and R.V. supervised human leukocyte experiments. P.Z. designed and conducted most *in vitro* experiments and drafted the manuscript. F.S. and A.P. collected human blood samples and patient data. Z.L., E.J. assisted with flow cytometry and data analysis. J.F. and Z.Y. performed the majority of *in vivo* experiments. A.S.Y., N.L., and C.L. prepared reagents and contributed to manuscript editing. B.M. and Y.M. generated TRPM2-KO mice. P.Z. and L.Y. wrote the manuscript, with input from all authors.

DECLARATION OF INTERESTS

The authors declare no competing interests.

STAR★METHODS

Detailed methods are provided in the online version of this paper and include the following:

- KEY RESOURCES TABLE
- METHOD DETAILS
  - Human individual enrollment
  - Human sample size and how subjects/samples were allocated to experimental groups
  - ELISA measurement of oxLDL and IL1β in plasma
  - Human peripheral blood leukocytes isolation and culture
  - Animals models
  - Middle cerebral artery occlusion (MCAO)
  - Neurological deficit score evaluation
  - Rotarod test
  - Evan's blue leakage assay after MCAO
  - Infarct volume assessment by triphenyl tetrazolium chloride (TTC) staining
  - Cerebral perfusion monitoring
  - Brain immune cell isolation and flow cytometry analysis
  - Mouse peripheral blood leukocytes isolation and culture
  - Bone marrow derived macrophages isolation and culture
  - Cerebral endothelial cells isolation and culture
  - Cortical neuron isolation and culture
  - *In vitro* endothelial barrier evaluation
  - Oxygen-glucose deprivation (OGD)
  - Use of antibodies, chemicals and reagents
  - Western blotting
- QUANTIFICATION AND STATISTICAL ANALYSIS
- ADDITIONAL RESOURCES

SUPPLEMENTAL INFORMATION

Supplemental information can be found online at https://doi.org/10.1016/j.xcrm.2025.101998.

Received: June 23, 2024
Revised: January 2, 2025
Accepted: February 11, 2025
Published: March 7, 2025

REFERENCES

1. Fredrickson, D.S. (1971). An international classification of hyperlipidemias and hyperlipoproteinemias. Ann. Intern. Med. *75*, 471–472. https://doi.org/10.7326/0003-4819-75-3-471.
2. Ballantyne, C.M., Grundy, S.M., Oberman, A., Kreisberg, R.A., Havel, R.J., Frost, P.H., and Haffner, S.M. (2000). Hyperlipidemia: diagnostic and therapeutic perspectives. J. Clin. Endocrinol. Metab. *85*, 2089–2112. https://doi.org/10.1210/jcem.85.6.6642-1.
3. Martone, A.M., Landi, F., Petricca, L., Paglionico, A., Liperoti, R., Cipriani, M.C., Ciciarello, F., Rocchi, S., Calvani, R., Picca, A., et al. (2022). Prevalence of dyslipidemia and hypercholesterolemia awareness: results from the Lookup 7+ online project. Eur. J. Publ. Health *32*, 402–407. https://doi.org/10.1093/eurpub/ckab224.
4. Menet, R., Bernard, M., and ElAli, A. (2018). Hyperlipidemia in Stroke Pathobiology and Therapy: Insights and Perspectives. Front. Physiol. *9*, 488. https://doi.org/10.3389/fphys.2018.00488.
5. Amarenco, P., Bogousslavsky, J., Callahan, A., 3rd, Goldstein, L.B., Hennerici, M., Rudolph, A.E., Sillesen, H., Simunovic, L., Szarek, M., Welch, K.M.A., et al. (2006). High-dose atorvastatin after stroke or transient ischemic attack. N. Engl. J. Med. *355*, 549–559. https://doi.org/10.1056/NEJMoa061894.
6. Campbell, B.C.V., De Silva, D.A., Macleod, M.R., Coutts, S.B., Schwamm, L.H., Davis, S.M., and Donnan, G.A. (2019). Ischaemic stroke. Nat. Rev. Dis. Primers *5*, 70. https://doi.org/10.1038/s41572-019-0118-8.
7. Narayan, S.K., Grace Cherian, S., Babu Phaniti, P., Babu Chidambaram, S., Rachel Vasanthi, A.H., and Arumugam, M. (2021). Preclinical animal studies in ischemic stroke: Challenges and some solutions. Animal Model. Exp. Med. *4*, 104–115. https://doi.org/10.1002/ame2.12166.
8. Guzik, A., and Bushnell, C. (2017). Stroke Epidemiology and Risk Factor Management. Continuum *23*, 15–39. https://doi.org/10.1212/CON.0000000000000416.
9. Maliougina, M., and El Hiani, Y. (2023). TRPM2: bridging calcium and ROS signaling pathways-implications for human diseases. Front. Physiol. *14*, 1217828. https://doi.org/10.3389/fphys.2023.1217828.
10. Zong, P., Lin, Q., Feng, J., and Yue, L. (2022). A Systemic Review of the Integral Role of TRPM2 in Ischemic Stroke: From Upstream Risk Factors to Ultimate Neuronal Death. Cells *11*, 491. https://doi.org/10.3390/cells11030491.
11. Zong, P., Li, C.X., Feng, J., Cicchetti, M., and Yue, L. (2024). TRP Channels in Stroke. Neurosci. Bull. *40*, 1141–1159. https://doi.org/10.1007/s12264-023-01151-5.
12. Zong, P., Feng, J., Yue, Z., Yu, A.S., Vacher, J., Jellison, E.R., Miller, B., Mori, Y., and Yue, L. (2022). TRPM2 deficiency in mice protects against atherosclerosis by inhibiting TRPM2-CD36 inflammatory axis in macrophages. Nat. Cardiovasc. Res. *1*, 344–360. https://doi.org/10.1038/s44161-022-00027-7.
13. Schierwagen, R., Maybüchen, L., Zimmer, S., Hittatiya, K., Bäck, C., Klein, S., Uschner, F.E., Reul, W., Boor, P., Nickenig, G., et al. (2015). Seven weeks of Western diet in apolipoprotein-E-deficient mice induce metabolic syndrome and non-alcoholic steatohepatitis with liver fibrosis. Sci. Rep. *5*, 12931. https://doi.org/10.1038/srep12931.
14. Pendse, A.A., Arbones-Mainar, J.M., Johnson, L.A., Altenburg, M.K., and Maeda, N. (2009). Apolipoprotein E knock-out and knock-in mice: atherosclerosis, metabolic syndrome, and beyond. J. Lipid Res. *50*, S178–S182. https://doi.org/10.1194/jlr.R800070-JLR200.
15. Syed Mortadza, S.A., Wang, L., Li, D., and Jiang, L.H. (2015). TRPM2 Channel-Mediated ROS-Sensitive Ca(2+) Signaling Mechanisms in Immune Cells. Front. Immunol. *6*, 407. https://doi.org/10.3389/fimmu.2015.00407.
16. Khan, I.M., Pokharel, Y., Dadu, R.T., Lewis, D.E., Hoogeveen, R.C., Wu, H., and Ballantyne, C.M. (2016). Postprandial Monocyte Activation in Individuals With Metabolic Syndrome. J. Clin. Endocrinol. Metab. *101*, 4195–4204. https://doi.org/10.1210/jc.2016-2732.
17. Short, J.D., Tavakoli, S., Nguyen, H.N., Carrera, A., Farnen, C., Cox, L.A., and Asmis, R. (2017). Dyslipidemic Diet-Induced Monocyte "Priming" and Dysfunction in Non-Human Primates Is Triggered by Elevated Plasma Cholesterol and Accompanied by Altered Histone Acetylation. Front. Immunol. *8*, 958. https://doi.org/10.3389/fimmu.2017.00958.
18. Kim, J., Park, K.T., Jang, M.J., Park, T.K., Lee, J.M., Yang, J.H., Song, Y.B., Choi, S.H., Gwon, H.C., Lee, S.H., et al. (2018). High-Intensity Versus Non-High-Intensity Statins in Patients Achieving Low-Density Lipoprotein Cholesterol Goal After Percutaneous Coronary Intervention. J. Am. Heart Assoc. *7*, e009517. https://doi.org/10.1161/JAHA.118.009517.
19. Ridker, P.M., Bhatt, D.L., Pradhan, A.D., Glynn, R.J., MacFadyen, J.G., Nissen, S.E., and PROMINENT REDUCE-IT and STRENGTH Investigators; and Investigators, S. (2023). Inflammation and cholesterol as predictors of cardiovascular events among patients receiving statin therapy: a collaborative analysis of three randomised trials. Lancet *401*, 1293–1301. https://doi.org/10.1016/S0140-6736(23)00215-5.
20. Ferroni, P., Martini, F., Cardarello, C.M., Gazzaniga, P.P., Davi, G., and Basili, S. (2003). Enhanced interleukin-1beta in hypercholesterolemia: effects of simvastatin and low-dose aspirin. Circulation *108*, 1673–1675. https://doi.org/10.1161/01.CIR.0000094732.02060.27.
21. Steinberg, D. (1997). Low density lipoprotein oxidation and its pathobiological significance. J. Biol. Chem. *272*, 20963–20966. https://doi.org/10.1074/jbc.272.34.20963.
22. Nagy, L., Tontonoz, P., Alvarez, J.G., Chen, H., and Evans, R.M. (1998). Oxidized LDL regulates macrophage gene expression through ligand activation of PPARgamma. Cell *93*, 229–240. https://doi.org/10.1016/s0092-8674(00)81574-3.
23. Pirillo, A., Norata, G.D., and Catapano, A.L. (2013). LOX-1, OxLDL, and atherosclerosis. Mediat. Inflamm. *2013*, 152786. https://doi.org/10.1155/2013/152786.
24. Lin, Y.Z., Yao, S.Y., Veach, R.A., Torgerson, T.R., and Hawiger, J. (1995). Inhibition of nuclear translocation of transcription factor NF-kappa B by a synthetic peptide containing a cell membrane-permeable motif and nuclear localization sequence. J. Biol. Chem. *270*, 14255–14258. https://doi.org/10.1074/jbc.270.24.14255.
25. Kang, K., Bachu, M., Park, S.H., Kang, K., Bae, S., Park-Min, K.H., and Ivashkiv, L.B. (2019). IFN-gamma selectively suppresses a subset of TLR4-activated genes and enhancers to potentiate macrophage activation. Nat. Commun. *10*, 3320. https://doi.org/10.1038/s41467-019-11147-3.
26. Shimizu, T., Dietz, R.M., Cruz-Torres, I., Strnad, F., Garske, A.K., Moreno, M., Venna, V.R., Quillinan, N., and Herson, P.S. (2016). Extended therapeutic window of a novel peptide inhibitor of TRPM2 channels following focal cerebral ischemia. Exp. Neurol. *283*, 151–156. https://doi.org/10.1016/j.expneurol.2016.06.015.
27. Gelderblom, M., Melzer, N., Schattling, B., Göb, E., Hicking, G., Arunachalam, P., Bittner, S., Ufer, F., Herrmann, A.M., Bernreuther, C., et al. (2014). Transient receptor potential melastatin subfamily member 2 cation channel regulates detrimental immune cell invasion in ischemic stroke. Stroke *45*, 3395–3402. https://doi.org/10.1161/STROKEAHA.114.005836.
28. Lory, N.C., Nawrocki, M., Corazza, M., Schmid, J., Schumacher, V., Bedke, T., Menzel, S., Koch-Nolte, F., Guse, A.H., Huber, S., and Mittrücker, H.W. (2021). TRPM2 Is Not Required for T-Cell Activation and Differentiation. Front. Immunol. *12*, 778916. https://doi.org/10.3389/fimmu.2021.778916.
29. Wang, Y., Leak, R.K., and Cao, G. (2022). Microglia-mediated neuroinflammation and neuroplasticity after stroke. Front. Cell. Neurosci. *16*, 980722. https://doi.org/10.3389/fncel.2022.980722.
30. Jiang, H., Zhou, Y., Nabavi, S.M., Sahebkar, A., Little, P.J., Xu, S., Weng, J., and Ge, J. (2022). Mechanisms of Oxidized LDL-Mediated Endothelial Dysfunction and Its Consequences for the Development of Atherosclerosis.

Front. Cardiovasc. Med. *9*, 925923. https://doi.org/10.3389/fcvm.2022.925923.

31. Steinberg, H.O., Bayazeed, B., Hook, G., Johnson, A., Cronin, J., and Baron, A.D. (1997). Endothelial dysfunction is associated with cholesterol levels in the high normal range in humans. Circulation *96*, 3287–3293. https://doi.org/10.1161/01.cir.96.10.3287.
32. Andjelkovic, A.V., Xiang, J., Stamatovic, S.M., Hua, Y., Xi, G., Wang, M.M., and Keep, R.F. (2019). Endothelial Targets in Stroke: Translating Animal Models to Human. Arterioscler. Thromb. Vasc. Biol. *39*, 2240–2247. https://doi.org/10.1161/ATVBAHA.119.312816.
33. Zong, P., Feng, J., Li, C.X., Jellison, E.R., Yue, Z., Miller, B., and Yue, L. (2024). Activation of endothelial TRPM2 exacerbates blood-brain barrier degradation in ischemic stroke. Cardiovasc. Res. *120*, 188–202. https://doi.org/10.1093/cvr/cvad126.
34. Rao, R. (2008). Oxidative stress-induced disruption of epithelial and endothelial tight junctions. Front. Biosci. *13*, 7210–7226. https://doi.org/10.2741/3223.
35. Yu, Q.J., Tao, H., Wang, X., and Li, M.C. (2015). Targeting brain microvascular endothelial cells: a therapeutic approach to neuroprotection against stroke. Neural Regen. Res. *10*, 1882–1891. https://doi.org/10.4103/1673-5374.170324.
36. ElAli, A., Doeppner, T.R., Zechariah, A., and Hermann, D.M. (2011). Increased blood-brain barrier permeability and brain edema after focal cerebral ischemia induced by hyperlipidemia: role of lipid peroxidation and calpain-1/2, matrix metalloproteinase-2/9, and RhoA overactivation. Stroke *42*, 3238–3244. https://doi.org/10.1161/STROKEAHA.111.615559.
37. de Oliveira, J., Engel, D.F., de Paula, G.C., Dos Santos, D.B., Lopes, J.B., Farina, M., Moreira, E.L.G., and de Bem, A.F. (2020). High Cholesterol Diet Exacerbates Blood-Brain Barrier Disruption in LDLr-/- Mice: Impact on Cognitive Function. J. Alzheimers Dis. *78*, 97–115. https://doi.org/10.3233/JAD-200541.
38. Saria, A., and Lundberg, J.M. (1983). Evans blue fluorescence: quantitative and morphological evaluation of vascular permeability in animal tissues. J. Neurosci. Methods *8*, 41–49. https://doi.org/10.1016/0165-0270(83)90050-x.
39. Honeycutt, S.E., and O'Brien, L.L. (2021). Injection of Evans blue dye to fluorescently label and image intact vasculature. Biotechniques *70*, 181–185. https://doi.org/10.2144/btn-2020-0152.
40. Li, J., Wang, P., Ying, J., Chen, Z., and Yu, S. (2016). Curcumin Attenuates Retinal Vascular Leakage by Inhibiting Calcium/Calmodulin-Dependent Protein Kinase II Activity in Streptozotocin-Induced Diabetes. Cell. Physiol. Biochem. *39*, 1196–1208. https://doi.org/10.1159/000447826.
41. Ostergaard, L., Jespersen, S.N., Mouridsen, K., Mikkelsen, I.K., Jonsdottir, K.Y., Tietze, A., Blicher, J.U., Aamand, R., Hjort, N., Iversen, N.K., et al. (2013). The role of the cerebral capillaries in acute ischemic stroke: the extended penumbra model. J. Cerebr. Blood Flow Metabol. *33*, 635–648. https://doi.org/10.1038/jcbfm.2013.18.
42. Keller, J.N., Hanni, K.B., and Markesbery, W.R. (1999). Oxidized low-density lipoprotein induces neuronal death: implications for calcium, reactive oxygen species, and caspases. J. Neurochem. *72*, 2601–2609. https://doi.org/10.1046/j.1471-4159.1999.0722601.x.
43. Zong, P., Feng, J., Yue, Z., Li, Y., Wu, G., Sun, B., He, Y., Miller, B., Yu, A.S., Su, Z., et al. (2022). Functional coupling of TRPM2 and extrasynaptic NMDARs exacerbates excitotoxicity in ischemic brain injury. Neuron *110*, 1944–1958.e8. https://doi.org/10.1016/j.neuron.2022.03.021.
44. Abdullah, S.M., Defina, L.F., Leonard, D., Barlow, C.E., Radford, N.B., Willis, B.L., Rohatgi, A., McGuire, D.K., de Lemos, J.A., Grundy, S.M., et al. (2018). Long-Term Association of Low-Density Lipoprotein Cholesterol With Cardiovascular Mortality in Individuals at Low 10-Year Risk of Atherosclerotic Cardiovascular Disease. Circulation *138*, 2315–2325. https://doi.org/10.1161/CIRCULATIONAHA.118.034273.
45. Abbate, A., Toldo, S., Marchetti, C., Kron, J., Van Tassell, B.W., and Dinarello, C.A. (2020). Interleukin-1 and the Inflammasome as Therapeutic Targets in Cardiovascular Disease. Circ. Res. *126*, 1260–1280. https://doi.org/10.1161/CIRCRESAHA.120.315937.
46. Uno, M., Kitazato, K.T., Nishi, K., Itabe, H., and Nagahiro, S. (2003). Raised plasma oxidised LDL in acute cerebral infarction. J. Neurol. Neurosurg. Psychiatry *74*, 312–316. https://doi.org/10.1136/jnnp.74.3.312.
47. Shimizu, T., Macey, T.A., Quillinan, N., Klawitter, J., Perraud, A.L.L., Traystman, R.J., and Herson, P.S. (2013). Androgen and PARP-1 regulation of TRPM2 channels after ischemic injury. J. Cerebr. Blood Flow Metabol. *33*, 1549–1555. https://doi.org/10.1038/jcbfm.2013.105.
48. Toda, T., Yamamoto, S., Umehara, N., Mori, Y., Wakamori, M., and Shimizu, S. (2019). Protective Effects of Duloxetine against Cerebral Ischemia-Reperfusion Injury via Transient Receptor Potential Melastatin 2 Inhibition. J. Pharmacol. Exp. Therapeut. *368*, 246–254. https://doi.org/10.1124/jpet.118.253922.
49. Wang, A., Yang, Y., Su, Z., Yue, W., Hao, H., Ren, L., Wang, Y., Cao, Y., and Wang, Y. (2017). Association of Oxidized Low-Density Lipoprotein With Prognosis of Stroke and Stroke Subtypes. Stroke *48*, 91–97. https://doi.org/10.1161/STROKEAHA.116.014816.
50. Yamamoto, S., Shimizu, S., Kiyonaka, S., Takahashi, N., Wajima, T., Hara, Y., Negoro, T., Hiroi, T., Kiuchi, Y., Okada, T., et al. (2008). TRPM2-mediated Ca2+influx induces chemokine production in monocytes that aggravates inflammatory neutrophil infiltration. Nat. Med. *14*, 738–747. https://doi.org/10.1038/nm1758.
51. Hoffman, N.E., Miller, B.A., Wang, J., Elrod, J.W., Rajan, S., Gao, E., Song, J., Zhang, X.Q., Hirschler-Laszkiewicz, I., Shanmughapriya, S., et al. (2015). Ca(2)(+) entry via Trpm2 is essential for cardiac myocyte bioenergetics maintenance. Am. J. Physiol. Heart Circ. Physiol. *308*, H637–H650. https://doi.org/10.1152/ajpheart.00720.2014.
52. Cheng, Y., Sudarov, A., Szulc, K.U., Sgaier, S.K., Stephen, D., Turnbull, D.H., and Joyner, A.L. (2010). The Engrailed homeobox genes determine the different foliation patterns in the vermis and hemispheres of the mammalian cerebellum. Development *137*, 519–529. https://doi.org/10.1242/dev.027045.
53. Schneider, C.A., Rasband, W.S., and Eliceiri, K.W. (2012). NIH Image to ImageJ: 25 years of image analysis. Nat. Methods *9*, 671–675. https://doi.org/10.1038/nmeth.2089.
54. Miller, B.A., Wang, J., Hirschler-Laszkiewicz, I., Gao, E., Song, J., Zhang, X.Q., Koch, W.J., Madesh, M., Mallilankaraman, K., Gu, T., et al. (2013). The second member of transient receptor potential-melastatin channel family protects hearts from ischemia-reperfusion injury. Am. J. Physiol. Heart Circ. Physiol. *304*, H1010–H1022. https://doi.org/10.1152/ajpheart.00906.2012.
55. Zong, P., Feng, J., Legere, N., Li, Y., Yue, Z., Li, C.X., Mori, Y., Miller, B., Hao, B., and Yue, L. (2024). TRPM2 enhances ischemic excitotoxicity by associating with PKCgamma. Cell Rep. *43*, 113722. https://doi.org/10.1016/j.celrep.2024.113722.

STAR★METHODS

KEY RESOURCES TABLE

REAGENT or RESOURCE	SOURCE	IDENTIFIER
Antibodies		
Rabbit polyclonal antibodies to TRPM2	Novus	Cat#NB110-81601; RRID: AB_1216361
Phospho-NF-κB p65 (Ser536) (93H1) Rabbit mAb	Cell Signaling Technology	Cat#3033; RRID: AB_331284
NF-κB p65 (D14E12) XP® Rabbit mAb	Cell Signaling Technology	Cat#8242; RRID: AB_10859369
CD36 (D8L9T) Rabbit mAb	Cell Signaling Technology	Cat#14347; RRID: AB_2798555
Caspase-1 (D7F10) Rabbit mAb	Cell Signaling Technology	Cat#3866; RRID: AB_10622129
IL-1β (D3U3E) Rabbit mAb	Cell Signaling Technology	Cat#12703; RRID: AB_2687927
Caspase-3 (D3R6Y) Rabbit mAb	Cell Signaling Technology	Cat#14220; RRID: AB_2687927
Occludin (E6B4R) Rabbit mAb	Cell Signaling Technology	Cat#91131; RRID: AB_2798555
iNOS (D6B6S) Rabbit mAb	Cell Signaling Technology	Cat#13120; RRID: AB_2687529
β-Tubulin Antibody	Cell Signaling Technology	Cat#2146; RRID: AB_2210370
GAPDH (D16H11) XP® Rabbit mAb	Cell Signaling Technology	Cat#5174; RRID: AB_10622025
HRP-linked anti-rabbit IgG	Cell Signaling Technology	Cat#7074S; RRID: AB_2099233
CD11b Monoclonal Antibody (M1/70), APC-eFluor™ 780, eBioscience™	Thermal Fisher Scientific	Cat#47-0112-82; RRID: AB_1603193
Alexa Fluor® 700 Rat Anti-Mouse Ly-6C	BD Biosciences	Cat#561237; RRID: AB_10612017
FITC anti-mouse Ly-6G Antibody	BioLegend	Cat#127605; RRID: AB_1236488
PE anti-mouse CD3ε Antibody	BioLegend	Cat#100308; RRID: AB_312673
CD19 Rat anti-Mouse, PerCP-Cy5.5, Clone: 1D3, BD	BD Biosciences	Cat#551001; RRID: AB_398497
APC anti-mouse CD45.2 Antibody	BioLegend	Cat#109814; RRID: AB_389210
Chemicals, peptides, and recombinant proteins		
DAPI (4′,6-Diamidino-2-Phenylindole, Dilactate)	BioLegend	Cat#422801
Tetrazolium chloride	Sigma-Aldrich	Cat#T-8877
Sulfosuccinimidyl Oleate (sodium salt)	Cayman chemical	Cat#11211
Mn(III)TBAP (chloride)	Cayman chemical	Cat#75850
L-NMMA (acetate)	Cayman chemical	Cat#10005031
SN50	Cayman chemical	Cat#17493
AP5	Cayman chemical	Cat#14539
MK-801	Sigma-Aldrich	Cat#M107
NP40	Thermal Fisher Scientific	Cat#28324
Triton™ X-100	Thermal Fisher Scientific	Cat#T-9284
Evans Blue	Sigma-Aldrich	Cat#E2129
Oxidized Low-density Lipoprotein (OxLDL)	Thermal Fisher Scientific	Cat#L34357
Low-Density Lipoprotein from Human Plasma (LDL)	Thermal Fisher Scientific	Cat#L3486
Penicillin-Streptomycin (10,000 U/mL)	Thermal Fisher Scientific	Cat#15140122
Poly-D-Lysine	Thermal Fisher Scientific	Cat#A3890401
B27 Supplement	Thermal Fisher Scientific	Cat#17504044
GlutaMAX™ Supplement	Thermal Fisher Scientific	Cat#35050061
Trypsin-EDTA (0.25%)	Thermal Fisher Scientific	Cat#25200072
Horse Serum, heat inactivated	Thermal Fisher Scientific	Cat#26050088
Neurobasal™ Plus Medium	Thermal Fisher Scientific	Cat#A3582901
Bovine Serum Albumin	Sigma-Aldrich	Cat#9048-46-8
Fetal Bovine Serum (FBS)	Thermal Fisher Scientific	Cat#A4766
Collagenase D	Sigma-Aldrich	Cat#11088882001
DNaseI	Sigma-Aldrich	Cat#10104159001

(*Continued on next page*)

Continued

REAGENT or RESOURCE	SOURCE	IDENTIFIER
Percoll®	Sigma-Aldrich	Cat#P1644
TAT-SC	Customed by Genescript	Sequence: YGRKKRRQRRRVILLKDHTLEYPVF
TAT-M2	Customed by Genescript	Sequence: YGRKKRRQRRRGSREPGEMLPRKLKRVLRQEFWV
Corning® Collagen I, Rat Tail B-27™	Corning	Cat#354236
Endothelial cell growth supplement from bovine neural tissue	Sigma-Aldrich	Cat#E2759-15MG
Macrophage Colony Stimulating Factor from mouse	Sigma-Aldrich	Cat#M9170-10UG
Critical commercial assays		
Mouse Transient Receptor Potential Cation Channel Subfamily M Member 2 (TRPM2) ELISA Kit	abbexa	Cat#abx551424
Pierce™ Rapid Gold BCA Protein Assay Kit	Thermal Fisher Scientific	Cat#A53225
Mouse Oxidized Low-Density Lipoprotein ELISA Kit	Abclonal	Cat#RK03096
LEGEND MAX™ Human IL-1β ELISA Kit	Biolegend	Cat#437007
Experimental models: Organisms/strains		
Non-inducible global TRPM2 knockout mouse strain (gM2KO)	Yamamoto et al.[50]	https://doi.org/10.1038/nm1758
Inducible global TRPM2 knockout mouse strain (*Trpm2$^{fl/fl}$*)	Nicholas et al.[51]	https://doi.org/10.1152/ajpheart.00720.2014
Global cre mouse strain (*Rosa26-cre^{ERT2}*)	Chen et al.[52]	https://doi.org/10.1242/dev.027045
Apoe$^{-/-}$ mouse strain	JAX	Cat#002052
Cd11b-cre mouse strain	JAX	Cat#019696
Cdh5-cre mouse strain	JAX	Cat#006137
*Apoe$^{-/-}$*gM2KO mouse strain	Zong et al. (2022a).[12]	https://doi.org/10.1016/j.neuron.2022.03.021
Trpm2$^{fl/fl}$Rosa26-cre^{ERT2} mouse strain	Zong et al. (2022b).[43]	https://doi.org/10.1016/j.neuron.2022.03.021
Apoe$^{-/-}$Trpm2$^{fl/fl}$Rosa26-cre^{ERT2} mouse strain	Zong et al. (2022a).[12]	https://doi.org/10.1038/s44161-022-00027-7
Trpm2$^{fl/fl}$Cd11b-cre mouse strain	Zong et al. (2022a).[12]	https://doi.org/10.1038/s44161-022-00027-7
Apoe$^{-/-}$Trpm2$^{fl/fl}$Cd11b-cre mouse strain	Zong et al. (2022a).[12]	https://doi.org/10.1038/s44161-022-00027-7
Trpm2$^{fl/fl}$Cdh5-cre mouse strain	Zong et al. (2024).[33]	https://doi.org/10.1093/cvr/cvad126
Apoe$^{-/-}$Trpm2$^{fl/fl}$Cdh5-cre mouse strain	Generated in this study	N/A
Software and algorithms		
ImageJ	Schneider et al.[53]	https://imagej.nih.gov/ij/
Olympus APEX 100 microscope and imaging system	N/A	https://evidentscientific.com/en/products/inverted/apexview
RFLSI-ZW Laser Speckle Contrast Imaging System and LSCI 6.0 software	N/A	https://www.rwdstco.com/product-item/rflsi-zw-laser-speckle-contrast-imaging-system/
FlowJo (9.9.6)	N/A	http://v9docs.flowjo.com/html/releasenotes.html
GraphPad Prism 9.0	N/A	https://www.graphpad.com/updates/prism-900-release-notes

METHOD DETAILS

Human individual enrollment

Institutional permissions and informed consent were obtained prior to conducting the study. The study was approved by the Office of Clinical & Translational Research (OCTR) at the University of Connecticut School of Medicine (IRB NUMBER: IE-13-119-2, Approval Date: 04/14/2022). All participants provided written informed consent before enrollment. Each participant was given a detailed explanation of the study's purpose, procedures, potential risks, and benefits before signing the consent form. If a participant was unable to provide consent at the time of enrollment, their legally authorized representative (LAR) was contacted as soon as feasible to review and sign the consent form on their behalf. If in-person consent was not possible, the consent documents were sent electronically or discussed over the phone, allowing the LAR sufficient time for review before providing signed authorization. A witness was also required to sign the consent form in cases of remote authorization. Additionally, all participants received a copy of the signed consent

form and HIPAA authorization, ensuring transparency regarding the use of their data and samples. The consent process adhered strictly to institutional ethical guidelines, and no data or biological samples were used without documented consent.

Human sample size and how subjects/samples were allocated to experimental groups

Our study includes a total of 66 enrolled human participants, categorized into four groups based on their blood LDL levels: optimal (<100 mg/dL), near optimal (100–129 mg/dL), borderline high (130–159 mg/dL), and high (>160 mg/dL). For correlation analyses, participants were analyzed as a continuous variable without predefined grouping.

ELISA measurement of oxLDL and IL1β in plasma

Plasma was collected during leukocyte isolation and frozen before ELISA experiments. Experiments were performed following the manufacturer's instructions for the oxLDL (Mouse Oxidized Low-Density Lipoprotein ELISA Kit, Abclonal, RK03096) and IL-1β (LEGEND MAX Human IL-1β ELISA Kit, BioLegend, 437007) kits. For IL-1β quantification, frozen plasma samples were thawed and added to pre-coated 96-well plates containing immobilized anti-human IL-1β antibodies. Standards and samples were incubated at room temperature for 2 h with gentle shaking, followed by extensive washing. A biotinylated detection antibody was then applied, followed by streptavidin-HRP, and incubated for an additional hour. After another wash step, TMB substrate was added to each well, and the reaction was stopped with an acidic solution. Optical density was measured at 450 nm using a microplate reader. For measuring oxLDL content in the brain, the entire hemisphere was weighed and manually homogenized in 1.5 mL of sample dilution buffer provided by the kit. The homogenate was transferred to a 2 mL centrifuge tube, incubated overnight in the cold room with shaking, and centrifuged at 12,000 g for 20 min. The supernatant was then collected and used for oxLDL quantification following the same ELISA protocol as for plasma samples.

Human peripheral blood leukocytes isolation and culture

All experimental procedures and analyses involving human blood cells were approved by the Office of Clinical & Translational Research (OCTR) at the University of Connecticut School of Medicine (IRB NUMBER: IE-13-119-2, Approval Date: 04/14/2022). Blood samples from de-identified human donors were centrifuged at 500 g for 10 min. Plasma was collected and frozen for the measurement of oxLDL and IL-1β levels. Red blood cell lysis buffer was added at a 5:1 ratio to the cell pellet, and the mixture was incubated at room temperature for 20 min, followed by centrifugation at 500*g* for 5 min. The resulting cell pellet was washed three times with PBS, each time centrifuging at 500 g for 5 min. The washed cells were either frozen for protein isolation or resuspended in DMEM/F12 supplemented with 10% FBS. The resuspended cells were plated on cell culture dishes pre-coated with poly-L-lysine for subsequent culture.

Animals models

All the experimental mice bred and hosted in the animal facility building of University of Connecticut School of Medicine (UCONN Health) were fed with standard chow diet and water *ad libitum*. Standard housing conditions were maintained at a controlled temperature with a 12-h light/dark cycle. All animal related experimental procedures and protocols were approved by the Institutional Animal Care and Use Committee (IACUC) of University of Connecticut School of Medicine (animal protocol: AP-200135-0723), and were conducted in accordance with the U.S. National Institutes of Health Guidelines for the Care and Use of Laboratory Animals.

The conventional global TRPM2 knockout (TRPM2-KO, or gM2KO) mice were generated by Dr. Yasuo Mori's lab at Kyoto University Japan.[50] The deletion of *Trpm2* was achieved by deleting the exon encoding the transmembrane segment 5 and part of the linker between segments 5 and 6 (S5–S6 linker in the pore domain).[50] The *Trpm2* deletion mice were backcrossed with C57BL6 mice for ≥10 generations before being used for experiments. The knockout mice exhibited no differences in behavior or impairment in breeding, compared to wild type (WT) C57BL/6 mice.

The conditional $Trpm2^{fl/fl}$ mice generated by Dr. Barbara Miller at the Pennsylvania State University College of Medicine, were used for inducible global and cell-type specific TRPM2 knockout. For generating inducible global TRPM2 KO mice, we used $Trpm2^{fl/fl}$ mice crossed with inducible global Cre mice, Rosa26-Cre^{ERT2} that were kindly provided by Dr. Joyner,[52] then the $Trpm2^{fl/fl}$-Rosa26-Cre^{ERT2} mice were further crossed with $Apoe^{-/-}$. The generation of myeloid cell specific TRPM2 knockout using *Cd11b-cre* mice[12] and endothelial cell specific TRPM2 knockout using *Cdh5-cre* mice[33] crossed with $Trpm2^{fl/fl}$ mice[54] were performed as we previously described.[12,33] The reason that we also used inducible global Cre crossed with $Trpm2^{fl/fl}$ mice to generate inducible global *Trpm2* deletion was to ensure that the global and cell-type specific TRPM2 knockout mice have comparable genetic background. Global and cell-type specific Cre^{+} and Cre^{-} $Trpm2^{fl/fl}$ mice were further crossed with $Apoe^{-/-}$ mice, and *Trpm2* deletion was induced by tamoxifen treatment for 5 days for the inducible cre mice one-week prior HFD treatment experiments.

Male mice aged 16 to 20 weeks were used in this study. After being fed a high-fat diet (HFD) for 4 to 5 months, the mice were at least 8 to 10 months old at the time of undergoing the MCAO procedure.

Middle cerebral artery occlusion (MCAO)

Nine-to ten-month-old male mice were subjected to transient middle cerebral artery occlusion (tMCAO) for 60 min followed by 24 h of reperfusion. The genotype information was blinded to the surgeon who conduct the surgeries. MCAO surgery was performed as previously described. In brief, mice were anesthetized based on animal protocol. The unilateral right middle cerebral artery (MCA)

occlusion was achieved by inserting a silicone-coated 6-0 monofilament (Doccol Corporation, Sharon, MA) 10 to 11 mm from internal carotid artery bifurcation via an external carotid artery incision. Mouse body temperature was maintained at ~37°C (TCA T-2DF, Physitemp). Cerebral blood flow was monitored before and after occlusion as well as after reperfusion. A reduction of 80%–90% in the peak systolic velocity (PSV) or mean flow velocity (MFV) is considered indicative of successful occlusion, while successful reperfusion after MCAO is confirmed when blood flow in the MCA returns to approximately 80–100% of pre-occlusion levels. The bregma was exposed and the skull bone countersunk at two 3 × 3-mm areas over both MCA supply territories for bilateral monitoring of local cortical blood flow. Successful occlusion was confirmed by 85% reduction of cerebral blood flow monitored using laser Doppler blood FlowMeter (Moor-VMS-LDF1, Moor Instrument, Dever, UK). Sham control mice underwent the same procedure but without insertion of filament to occlude the MCA. The detailed blood flow information of different group of mice are summarized in Table S1.

Neurological deficit score evaluation

Neurological deficit was scored based on previously reported criteria.[33,43,55] In brief, score 0 represents no neurological deficit; score 1 represents failure to extend left paw; Score 2 represents circling to the left; score 3 represents falling to the left; score 4 represents inability of spontaneously walking and decreased level of consciousness; and score 5 represents death due to brain ischemia. The observer to score the neurological deficit was an experienced observer and blinded by the group assignment and genotype information. If the animal score was 0 or 5, it was removed from the study.

Rotarod test

For examining the long-term protective effect of TAT-M2, motor coordination of mice was evaluated by rotarod test right after the evaluation of neurological deficit score at 1st, 3rd, and 7th day after MCAO. Briefly, mice were placed on a rotating rod with the speed range of 6–56 rounds per minute for 5 min. Each mouse was tested for 3 times with two 20-min interval in between. The falling from the rotating rod was recorded and the averaged latency of each mouse was used for quantification.

Evan's blue leakage assay after MCAO

Evans blue measurement was performed according to a previously reported method.[33] Briefly, Evans blue was freshly prepared by dissolving it in PBS to a concentration of 2% prior to use. At 23 h after MCAO or sham surgery, approximately 100 μL of 2% Evans blue was injected intravenously into the mice. After 1 h, the mice were anesthetized with isoflurane and perfused intracardially with 10 mL of PBS. The brains were then removed, separated into hemispheres ipsilateral and contralateral to the MCAO side, and cut into 100 μm-thick slices using a vibratome. The slices were mounted onto slides for examining Evans blue emission at 680 nm using an Olympus APEX 100 microscope system. The size of the patchy Evans blue leakage area and the average Evans blue intensity in the ipsilateral hemisphere compared to the contralateral hemisphere were measured using ImageJ software. After overexposing the Evans blue fluorescence images, the brain microvasculature was visualized, and quantification of capillary density, capillary length, capillary branching, and capillary tortuosity index was performed using ImageJ.

For quantification of the Evans blue content in the brain using colorimetry,[33] brain slices from each hemisphere were homogenized in 0.4 mL N,N-dimethylformamide (Sigma-Aldrich, DX1730) and centrifuged for 60 min at 18,000 rcf. The supernatants were collected, and absorbance was measured at 500 nm, 620 nm, and 740 nm. Evans blue levels in the brain were calculated using the following formula: (A620nm – ((A500nm + A740nm)/2))/mg (wet weight) as we previously reported.[33]

Infarct volume assessment by triphenyl tetrazolium chloride (TTC) staining

Tetrazolium chloride (Sigma-Aldrich, T-8877) was dissolved in PBS at a concentration of 2% 30 min prior to use. Post-stroke mice were euthanized, and brains were frozen at −80°C for 5 min. Brains were cut into coronary slices at a thickness of 1 mm. Brain slices were stained with 2% TTC (vol/vol) for 20 min, and then washed using PBS for 3 times, and fixed in *10% Neutral* buffered *formalin* for later scanning. TTC labels non-injured tissue, leaving the infarct area white. The stained slices were scanned for data analysis using ImageJ software. The infarct volume was calculated and presented as a percentage of total brain volume as previously reported.

Cerebral perfusion monitoring

RFLSI-ZW Laser Speckle Contrast Imaging System (RWD) were used to monitor the cerebral blood perfusion based on a previously reported protocol and manufacturer's instruction. Laser speckle blood flow images were recorded and used to identify the regions of interest (ROIs). Within these ROIs, the mean blood flow index was calculated, and a relative CBF was determined by calculating the ratio of the ipsilateral CBF to that of the corresponding contralateral area. Collected data was analyzed using LSCI 6.0 software (RWD).

Brain immune cell isolation and flow cytometry analysis

Brains were harvested 24 h after MCAO following an extensive perfusion with 10 mL of heparinized PBS to remove the blood in the brains. Then brain hemispheres were minced thoroughly using a micro-scissor. Collagenase D (Sigma, 11088882001) at 1.6 mg/mL with DNaseI (Sigma, 10104159001) at 666 U/ml in HBSS with 2 mM Ca^{2+} and 2 mM Mg^{2+} were used for digestion. Minced brain

tissues were transferred into digestion buffer (3 mL per hemisphere), and digested in a water bath shaker at 37°C for 56 min. After the digestion, tissue suspensions were pipetted up and down using a P1000, filtered through a 30 μm cell strainer, and centrifuge at 366 g for 6 min. Then 25% Percoll (Sigma, P1644) (5 mL per hemisphere) was used to separate and remove the myelin debris by centrifuging the resuspensions at 666 g for 16 min. The cell pellets were resuspended and washed using PBS with 5% FBS, and were ready for antibody staining and flow cytometry analysis as we reported before. Flow cytometry was performed using ZE5 Cell Analyzer (BIO-RAD). Collected data were analyzed using FlowJo (9.9.6). Singlets were chosen from the scatter gate, from which alive cells were separated by DAPI. CD45 was used to distinguish infiltrated leukocytes ($CD45^{high}$) and microglia ($CD45^{medium}$). In the leukocytes gate,[12] myeloid cells and lymphocytes were separated based on cell size. Ly6G was used to separate neutrophils from the monocytes/macrophages, which were further characterized using CD11b and Ly6C. Lymphocytes were characterized using CD3e and CD19 to distinguish T cells and B cells, respectively. Microglia populations were characterized using CD11b and Ly6C.

Mouse peripheral blood leukocytes isolation and culture

Blood samples from mice were centrifuged at 500 g for 10 min. Plasma was collected and frozen for the measurement of oxLDL and IL-1β levels. Red blood cell lysis buffer was added at a 5:1 ratio to the cell pellet, and the mixture was incubated at room temperature for 20 min, followed by centrifugation at 500*g* for 5 min. The resulting cell pellet was washed three times with PBS, each time centrifuging at 500 g for 5 min. The washed cells were either frozen for protein isolation or resuspended in DMEM/F12 supplemented with 10% FBS. The resuspended cells were plated on cell culture dishes pre-coated with poly-L-lysine for subsequent culture.

Bone marrow derived macrophages isolation and culture

Mice were euthanized based on our IACUC-approved protocol, and femurs were quickly removed. Two ends of femurs were cut using scissors, and bone marrow was washed out using PBS. The collected bone marrow was thoroughly resuspended with macrophage culture medium: DMEM: Nutrient Mixture F-12 (DMEM/F12) (Thermal Fisher Scientific, 11330) supplemented with 25 ng/mL Macrophage Colony Stimulating Factor from mouse (Sigma, M9170-10UG), 10% BGS (HyClone, SH30541.03) and 0.5% penicillin/streptomycin (Thermal Fisher Scientific, 15140-122). Culture medium was changed every 3 days. After culturing for 7 days, macrophages were used for experiments.

Cerebral endothelial cells isolation and culture

Endothelial culture medium was made prior to isolation: DMEM/F12 (Thermal Fisher Scientific, 11330) was supplemented with 100 μg/mL endothelial cell growth supplement from bovine neural tissue (Sigma, E2759-15MG), 10% Fetal Bovine Serum (FBS) (Thermal Fisher Scientific, A4766) and 0.5% penicillin/streptomycin (Thermal Fisher Scientific, 15140-122).

Mice were euthanized following IACUC-approved protocols. The heads were quickly removed, and the brains were carefully extracted. On ice, the brains were dissected to remove the brainstem, cerebellum, and thalamus, then rolled on sterilized filter paper to remove the meninges. The brain tissue was then cut into small pieces suitable for pipetting with 1 mL pipette tips. The fragmented brain tissue was transferred into 12 mL of DMEM/F12 containing 300 U DNase I (Qiagen, 79254) and 12 mg collagenase II (Worthington, 4177), sufficient for digesting one brain. The mixture was thoroughly mixed and digested in a pre-warmed water bath shaker at 37°C for 1 h. After digestion, the homogenate was centrifuged at 1000 g for 10 min at 4°C. The supernatant was carefully removed, and the cell pellet was resuspended in 20% BSA in DMEM/F12 and centrifuged again at 1000 g for 20 min at 4°C. The supernatant was removed, and the cell pellet was resuspended in pre-warmed endothelial cell culture medium. The isolated cells from one brain were plated onto a 35 mm culture dish pre-coated with Corning Collagen I, Rat Tail (Corning, 354236). After 24 h, the medium was replaced, and puromycin was added at a concentration of 2 μg/mL (Sigma, P8833-25MG). The culture medium was replaced every 2 days, with puromycin added during the first week to inhibit the growth of non-endothelial cells. Immunofluorescence staining of CD31 was performed to confirm the purity of the isolated cerebral endothelial cells. Treatments and experiments were conducted after 2 weeks of culture.

Cortical neuron isolation and culture

Mice pups at P0 were euthanized based on animal protocol. Whole brain was harvested and immersed in frozen Hank's Balanced Salt Solution (HBSS). Meninges were peeled. Brain stem and thalamus were removed. Cortical tissues were cut into small pieces and digested with 0.25% trypsin (Thermal Fisher Scientific, 15090-046) in HBSS at 37°C for 15 min. Tissue pellets are washed with HBSS. Cells were resuspended with appropriate amount of Neurobasal Medium (Thermal Fisher Scientific, 21103-049) supplemented with 2% B27 supplement (Thermal Fisher Scientific, 17504-044), 3% horse serum (Thermal Fisher Scientific, 16050114), 0.25% L-glutamine (Thermal Fisher Scientific, 25030-081) and 1% penicillin/streptomycin (Thermal Fisher Scientific, 15140-122). Isolated cells were counted and plated on coverslips pre-coated with poly-L-lysine (Sigma-Aldrich, P4707) at a density of about 500 x 10^3 cells/cm^2 for OGD and H_2O_2 treatment, and 100 x 10^3 cells/cm^2 for current recording. Cytosine arabinoside (Sigma-Aldrich, C1768) was added to maintain a concentration at 1μM to inhibit the proliferation of non-neuronal cells. 24 h after plating, culture medium was changed to Neurobasal Medium supplemented with 2% B27 supplement, 0.25% L-glutamine and 1% penicillin/streptomycin. The concentration of Cytosine arabinoside (araC) was increased to 2 μM. Medium was changed every 3 days. Different treatments and experiments were performed at 7^{th} day of culture.

In vitro endothelial barrier evaluation

We measured endothelial barrier as we previously reported.[33] In brief, for the giga-seal leakage assay, we used our patch-clamp equipment, placing the recording electrode in the upper chamber of a transwell insert and the grounding electrode in the lower chamber, while CECs were plated on the insert for 3 to 5 days to allow them to form tight barriers. In the control groups, the barrier formed by the CECs was so tight that even ions could not freely exchange between the two chambers, creating a condition similar to the giga-seal observed in patch-clamp recordings. However, after OGD treatment, the integrity of the CEC barrier was compromised, allowing ions to freely pass between the two chambers and resulting in the loss of the giga-seal, which was monitored at different time points.

For the Evans blue leakage assay, CECs were plated on transwells with a 0.4 μm pore size (Thermo Fisher Scientific, 140620). CECs were cultured for 3 to 5 days until they completely covered the upper surface of the transwells, after which they were subjected to OGD treatment at different time points. Evans blue was dissolved in prewarmed HBSS at a concentration of 0.25% with 5% BSA. The Evans blue solution was then added to the upper chamber, and the culture medium in the lower chamber was replaced with HBSS. The cells were returned to the incubator for 10 min to allow Evans blue to diffuse into the lower chamber. HBSS from the lower chamber was subsequently collected, and absorbance was measured at 610 nm. For quantification, the absorbance value in the OGD or TSP1 treatment group was normalized to the absorbance value in the control group.

Oxygen-glucose deprivation (OGD)

Oxygen-glucose deprivation (OGD) was achieved by replace the glucose in Tyrode solution with sucrose, and 95% N2 and 5% CO2 was used to equilibrate sucrose-Tyrode solution to displace oxygen. This condition typically yielded a pO2 of <5 mm Hg in the imaging chamber. At least 10 min was allowed for endothelial cells to adapt to the change from culture medium to Tyrode solution before OGD was applied. Incubation time of OGD for cell culture and protein isolation was 4 h. For current recording and real-time cell imaging, OGD was achieved by bubbling sucrose-Tyrode solution with 95% N2 and 5% CO2.

Use of antibodies, chemicals and reagents

Rabbit polyclonal antibodies to TRPM2 (Novus, NB110-81601, 1:200 in 5% BSA for WB); Phospho-NF-κB p65 (Ser536) (93H1) Rabbit mAb (Cell Signaling Technology, 3033, 1:2000 in 5% BSA for WB); NF-κB p65 (D14E12) XP Rabbit mAb (Cell Signaling Technology, 8242, 1:2000 in 5% BSA for WB); CD36 (D8L9T) Rabbit mAb (Cell Signaling Technology, 14347, 1:2000 in 5% BSA for WB); Caspase-1 (D7F10) Rabbit mAb (Cell Signaling Technology, 3866, 1:2000 in 5% BSA for WB); IL-1β (D3U3E) Rabbit mAb (Cell Signaling Technology, 12703, 1:2000 in 5% BSA for WB); Caspase-3 (D3R6Y) Rabbit mAb (Cell Signaling Technology, 14220, 1:2000 in 5% BSA for WB); Occludin (E6B4R) Rabbit mAb (Cell Signaling Technology, 91131, 1:2000 in 5% BSA for WB); iNOS (D6B6S) Rabbit mAb (Cell Signaling Technology, 13120, 1:2000 in 5% BSA for WB); β-Tubulin Antibody (Cell Signaling Technology, 2146, 1:2000 in 5% BSA for WB); GAPDH (D16H11) XP Rabbit mAb (Cell Signaling Technology, 5174, 1:2000 in 5% BSA for WB); HRP-linked anti-rabbit IgG (Cell Signaling Technology, 7074S, 0.1 μg/mL in 5% BSA for WB); CD11b Monoclonal Antibody (M1/70), APC-eFluor 780, eBioscience (Thermal Fisher Scientific, 47-0112-82, 1:100 in 3% FBS for FC); Alexa Fluor 700 Rat Anti-Mouse Ly-6C (BD Biosciences, 561237, 1:100 in 3% FBS for FC); FITC anti-mouse Ly-6G Antibody (BioLegend, 127605, 1:100 in 3% FBS for FC); PE anti-mouse CD3ε Antibody (BioLegend, 100308, 1:100 in 3% FBS for FC); CD19 Rat anti-Mouse, PerCP-Cy5.5, Clone: 1D3, BD (BD Biosciences, BDB551001, 1:100 in 3% FBS for FC); APC anti-mouse CD45.2 Antibody (BioLegend, 109814, 1:100 in 3% FBS for FC); DAPI (4′,6-Diamidino-2-Phenylindole, Dilactate, 1 ng/mL in 3% FBS for FC) (BioLegend, 422801); Tetrazolium chloride (Sigma-Aldrich, T-8877); Oxidized Low-density Lipoprotein (OxLDL) (Thermal Fisher Scientific, L34357); Low-Density Lipoprotein from Human Plasma (LDL) (Thermal Fisher Scientific, L3486); Endothelial cell growth supplement from bovine neural tissue (Sigma, E2759-15MG); Macrophage Colony Stimulating Factor from mouse (Sigma, M9170-10UG); Corning Collagen I, Rat Tail B-27 (Corning, 354236); Penicillin-Streptomycin (10,000 U/mL) (Thermal Fisher Scientific, 15140122); Poly-D-Lysine (Thermal Fisher Scientific, A3890401); B27 Supplement (Thermal Fisher Scientific, 17504044); GlutaMAX Supplement (Thermal Fisher Scientific, 35050061); Trypsin-EDTA (0.25%) (Thermal Fisher Scientific, 25200072); Horse Serum, heat inactivated (Thermal Fisher Scientific, 26050088); Neurobasal Plus Medium (Thermal Fisher Scientific, A3582901); Sulfosuccinimidyl Oleate (sodium salt) (Cayman chemical, 11211); Mn(III)TBAP (chloride) (Cayman chemical, 75850); L-NMMA (acetate) (Cayman chemical, 10005031); SN50 (Cayman chemical, 17493); AP5 (Cayman chemical, 14539); MK-801 (Sigma-Aldrich, M107); NP40 (Thermal Fisher Scientific, 28324); Triton X-100 (T-9284), Bovine Serum Albumin (Sigma-Aldrich, 9048-46-8); Fetal Bovine Serum (FBS) (Thermal Fisher Scientific, A4766); Evans Blue (Sigma-Aldrich, E2129); Mouse Transient Receptor Potential Cation Channel Subfamily M Member 2 (TRPM2) ELISA Kit (abbexa, abx551424); TAT-SC and TAT-M2 were synthesized by Genescript.

Western blotting

NP-40/Triton lysis buffer (10% NP40, 1% Triton X-100, 150 mM NaCl, 1 mM EDTA, 50 mM Tris, pH = 8.0) containing proteinase inhibitors and phosphatase inhibitors was used to lyse PBMCs, cultured cells and frozen brain tissue. Cell and tissue lysate were lysed by ultrasound using an ultrasonic cleaner filled with ice-cold water for 30 min. After incubated on ice for 1 h, lysate was centrifuged at 13000 g for 30 min and supernatant was collected. Protein concentration was measured using Pierce Rapid Gold BCA Protein Assay Kit. 30–50 μg of total protein was loaded and separated proteins were transferred to Nitrocellulose membranes. Membranes were blocked with 5% BSA and 2.5% goat serum in Tris-buffered saline (TBS, pH = 7.4) at room temperature for 2 h, and incubated with primary antibodies in TBS with 0.05% Tween (TBS-T) at room temperature for 2 h. Then membranes were incubated with

secondary antibodies in TBS-T for 1 h at room temperature for 1 h for detection. Blots were developed with ImageQuant LAS 4000 imaging system. Band intensity was quantified using ImageJ software and normalized with appropriate loading controls.

QUANTIFICATION AND STATISTICAL ANALYSIS

All data are expressed as mean ± standard error of the mean (SEM) and "n" is the number of biological replicates. Experiments were repeated at least three times. Sample size was estimated by Power analysis using the webtool7 (https://clincalc.com/stats/samplesize.aspx), or G*Power software (http://www.gpower.hhu.de/), which utilize independent study groups, type I error α = 0.05 and power = 80%. Randomization was used to divide animals or experimental samples into separated groups that compare different treatments to avoid bias in all our experiments. Random assignment subjects to different treatment groups was performed using GraphPad "Random number calculators" to assign subjects to different groups. GraphPad Prism v9 (GraphPad Software, Inc.) was also used for statistical analyses. Data quantification and analysis were performed blindly. Prior to statistical analysis, data were analyzed for normality by Kolmogorov-Smirnov test or Shapiro-Wilk test as a justification for using Student's t-test or analysis of variance (ANOVA). Equal variance was analyzed using Bartlett test and F-test for multiple comparison groups and two-sample t-test respectively. If normality and equal variance were not satisfied, Mann-Whitney test was used for statistical analysis for two groups' comparison and Kruskal-Wallis non-parametric test, with Dun's multiple comparison, was used for comparison between multiple groups as previously reported7. In GraphPad Prism 9.0, Welch's ANOVA and Brown-Forsythe ANOVA also automatically adjusts the calculations of the F ratio and degrees of freedom to adjust for heterogeneity of within-group variances. The p value can be interpreted in the same manner as in the analysis of variance. For two groups' comparison, statistical significance was determined using two-tailed Student's t test. For multiple groups, statistical significance was determined using one-way or two-way ANOVA, followed by Bonferroni post-test with correction. One-way ANOVA was used for comparison of multiple groups with one variable, and two-way ANOVA was used when there were two independent variables. Two-sided $p < 0.05$ was considered statistically significant. The sample size for Western blot experiments means six dishes of cells from at least two mice. The sample size for live cell imaging experiments means 20–40 cells from at least three dishes of cells, which were collected from more than two mice (also see Figure legend).

ADDITIONAL RESOURCES

Any additional information required to replicate the experiments in this work paper is available from the lead contact upon request.

The collection of human peripheral leukocytes for our study is linked to the registered clinical trial NCT04321512, titled *Study of Circulating Monocytes in Patients with Ischemic Vascular Disease*, available at ClinicalTrials.gov.